ผลของสภาวะการเผาที่มีต่อสมบัติของผลึกและค่าความว่องไวในการเร่งปฏิกิริยาโดยใช้แสงของไทเทเนียมไดออกไซด์ และของผสมระหว่าง ไทเทเนียมไดออกไซด์และออกไซด์ของธาตุหมู่ IVA และ IVB

นางสาวรัชฎาภรณ์ นิลเพชร

วิทยานิพนธ์นี้เป็นส่วนหนึ่งของการศึกษาตามหลักสูตรปริญญาวิศวกรรมศาสตรมหาบัณฑิต
สาขาวิชาวิศวกรรมเคมี ภาควิชาวิศวกรรมเคมี
คณะวิศวกรรมศาสตร์ จุฬาลงกรณ์มหาวิทยาลัย
ปีการศึกษา 2547

ISBN 974-53-1422-6

EFFECT OF CALCINATION CONDITIONS ON PROPERTIES AND PHOTOCATALYTIC ACTIVITIES OF TITANIUM DIOXIDE AND MIXTURES OF TITANIUM DIOXIDE AND OXIDE OF GROUP IVA AND IVB ELEMENTS

Miss Ratchadaporn Ninpetch

A Thesis Submitted in Partial Fulfillment of the Requirements
for the Degree of Master of Engineering in Chemical Engineering
Department of Chemical Engineering
Faculty of Engineering
Chulalongkorn University
Academic Year 2004

ISBN 974-53–1422-6

Thesis Title	EFFECT OF CALCINATION CONDITIONS ON PROPERTIES AND PHOTOCATALYTIC ACTIVITIES OF TITANIUM DIOXIDE AND MIXTURES OF TITANIUM DIOXIDE AND OXIDE OF GROUP IVA AND IVB ELEMENTS
By	Miss Ratchadaporn Ninpetch
Field of Study	Chemical Engineering
Thesis Advisor	Akawat Sirisuk, Ph.D.

Accepted by the Faculty of Engineering, Chulalongkorn University in Partial Fulfillment of the Requirements for the Master's Degree

…… ...Dean of the Faculty of Engineering
(Professor Direk Lavansiri, Ph.D.)

THESIS COMMITTEE

……Chairman
(Associate Professor Suttichai Assabumrungrat, Ph.D.)

…….. Thesis Advisor
(Akawat Sirisuk, Ph.D.)

……. Member
(Waraporn Tanakulrungsank, D.Eng.)

…….Member
(Joongjai Panpranot, Ph.D.)

รัชฎาภรณ์ นิลเพชร: ผลของสภาวะการเผาที่มีต่อสมบัติของผลึกและค่าความว่องไวในการเร่งปฏิกิริยาโดยใช้แสงของไทเทเนียมไดออกไซด์ และของผสมระหว่าง ไทเทเนียมไดออกไซด์ และออกไซด์ ของธาตุหมู่ IVA และ IVB (EFFECT OF CALCINATION CONDITIONS ON PROPERTIES AND PHOTOCATALYTIC ACTIVITIES OF TITANIUM DIOXIDE AND MIXTURES OF TITANIUM DIOXIDE AND OXIDE OF GROUP IVA AND IVB ELEMENTS) อ. ที่ปรึกษา: ดร.อัครวัต ศิริสุข, 84 หน้า, ISBN: 974–53–1422-6

ไทเทเนียที่ใช้เป็นตัวเร่งในปฏิกิริยาออกซิเดชั่นของเอทิลีนนั้นมีขนาดเล็กอยู่ในระดับนาโนเมตร สามารถเตรียมได้โดยวิธีโซล-เจล โดยใช้ ไทเทเนียมไอโซโพรพรอกไซด์เป็นสารตั้งต้น ผ่านการเผาที่อุณหภูมิ และเวลาที่แตกต่างกัน การทดสอบคุณลักษณะของไทเทเนียนั้น ทำการศึกษาโดยใช้ การกระเจิงรังสีเอ๊กซ์ เอ๊กซ์อาร์เอฟ เอฟทีไออาร์ และการวัดพื้นที่ผิว การศึกษาผลของสภาวะในการเผา ซึ่งได้แก่ อุณหภูมิ และเวลาที่ใช้ในการเผา ที่มีผลต่อคุณสมบัติ และค่าความว่องไวของการเกิดปฏิกิริยาของไทเทเนีย ผลการศึกษาพบว่าไทเทเนียที่เผาที่อุณหภูมิ 200 องศาเซลเซียสเป็นเวลา 1 ชั่วโมง ให้ค่าความว่องไวในการเกิดปฏิกิริยาสูงที่สุด เพราะว่ามีพื้นที่ผิวสูง และไม่มีเฟสของรูไทล์ผสมอยู่ ส่วนการศึกษาผลของการเติมโลหะออกไซด์ตัวที่สองเช่น ซิลิกา เซอร์โครเนีย ทินไดออกไซด์ และซีเรีย จำนวน 10 เปอร์เซ็นต์โดยน้ำหนัก ลงในไทเทเนีย เพื่อให้กลายเป็นของผสมออกไซด์ และนำไปเผาที่อุณหภูมิ 200 องศาเซลเซียสเป็นเวลา 1 ชั่วโมง ที่มีต่อค่าความว่องไวของการเกิดปฏิกิริยา พบว่าการเติมโลหะออกไซด์ตัวที่สองลงไปจะทำให้ค่าความว่องไวของการเกิดปฏิกิริยาต่ำกว่าของไทเทเนียที่ไม่มีการเติมโลหะออกไซด์อื่น

ภาควิชา.... ...วิศวกรรมเคมี..... ลายมือชื่อนิสิต.....

สาขาวิชา.....วิศวกรรมเคมี..... ลายมือชื่ออาจารย์ที่ปรึกษา.....

ปีการศึกษา.... .2547.....

##4670452121: MAJOR CHEMICAL ENGINEERING
KEY WORD: TITANIA / TITANIUM (IV) OXIDE / SOL-GEL METHOD / RUTILE CONTENT / SILICA/ ZIRCONIA/ CERIA/ TIN DIOXIDE/ PHOTOCATALYTIC OXIDATION OF ETHYLENE

RATCHADAPORN NINPETCH: EFFECT OF CALCINATION CONDITIONS ON PROPERTIES AND PHOTOCATALYTIC ACTIVITIES OF TITANIUM DIOXIDE AND MIXTURES OF TITANIUM DIOXIDE AND OXIDE OF GROUP IVA AND IVB ELEMENTS THESIS ADVISOR: AKAWAT SIRISUK, Ph.D. 84 pp. ISBN 974-53-1422-6

Titania nanoparticles were prepared via a sol-gel method using titanium isopropoxide as a precursor and underwent calcination at various conditions. Titania was evaluated for its photocatalytic activity in photocatalytic oxidation of ethylene in gas phase. Various characterization techniques, including XRD, XRF, FT-IR and nitrogen adsorption, were employed. Effects of calcination conditions, namely, temperature and holding time in the furnace, on properties of titania nanoparticles were investigated. Titania that was calcined at 200°C for one hour exhibited the highest photocatalytic activity because of its large specific surface area and absence of rutile phase in the photocatalyst. Four different metal oxides, namely, SiO_2, ZrO_2, SnO_2, and CeO_2, were added to TiO_2 to form binary metal oxides. The amount of second metal oxide added was 10 wt%. The mixed oxides were calcined at 200°C for one hour and were then tested for activities. Addition of the second metal oxide appeared to lower photocatalytic activity of the photocatalyst, when compared to that of pure titania.

Department.....Chemical Engineering….. Student's signature……...
Field of study….Chemical Engineering….. Advisor's signature……
Academic year…2004…….....

ACKNOWLEDGEMENTS

This dissertation would not have been possible to complete without the support of the following individuals. Firstly, I would like to express my greatest gratitude to my advisor, Dr. Akawat Sirisuk, for his invaluable guidance during the course of this work, and I am also very grateful to Professor Dr. Piyasan Praserthdam, for his kind supervision over this thesis. Special thanks to Associate Professor Suttichai Assabumrungrat, as the chairman, Dr. Waraporn Tanakulrungsank and Dr. Joongjai Panpranot, members of the thesis committee for their kind cooperation.

The financial supports from the National Research Council (NRC), the Thailand Reserch Fund (TRF), TJTTP-JBIC and Graduate School of Chulalongkorn University are also gratefully acknowledged.

Many thanks for kind suggestions and useful help to Miss Patta Soisuwan and many friends in the Research Center on Catalysis and Catalytic Reaction Engineering who always provide the encouragement and assistance along the thesis study.

Finally, I also would like to dedicate this thesis to my parents and my brother who have always been the source of my support and encouragement.

CONTENTS

Page

Page

Page

LIST OF TABLES

LIST OF FIGURES

Figure **Page**

Figure **Page**

CHAPTER I

INTRODUCTION

Heterogeneous photocatalytic oxidation is a promising technique for the degradation of volatile organic compounds (VOCs) (Maira *et al*., 2001). Since it allows the oxidation of airbone VOCs into carbon dioxide and water at room temperature in the presence of a semiconductor photocatalyst (*e.g*., TiO_2) and UV or near-UV light source. The basic principle of semiconductor photocatalysis involves the migration of photogenerated electrons and holes to catalyst surfaces where they can react with adsorbed reactants, leading to the decomposition of pollutants. The photocatalytic oxidation of ethylene using TiO_2 (titania) catalyst has been studied by several researchers (Sirisuk *et al.*,1999; Fu *et al*.,1996; Park *et al.*, 1999) who observed different catalyst activities and efficiencies for TiO_2 that was prepared differently.

TiO_2 has been extensively used in solar energy conversion and photocatalysis because of its high photocatalytic activity, stability, suitable band-gap energy and so on (Kominami *et al.*, 2001). Moreover, these properties are dictated to a large extent by its crystal phase, morphology and particle size. In recent years, researchers have synthesized a variety of nanosized TiO_2 materials as nano-particles, nano-wires and so on. TiO_2 has three crystal phases: anatase, rutile and brookite (Hoffmann *et al.*, 1995; Linsebigler *et al.*, 1995) but anatase phase is generally more chemically and optically active. Crystal structures of titania can be controlled by heat treatment and sometimes by addition of dopants (Calza *et al.*, 1997; Mills and wang, 1997; Nam and Han, 2003). Titania that has nanocrystallite size and high surface area has attracted interest due to the unusual photocatalytic properties; However, nanosized TiO_2 has a strong tendency to agglomerate to larger particles, leading to a decrease of thermal stability and exerting an influence on its applications.

The preparation of TiO_2 nanoparticles has been investigated using various methods, including vapor decomposition, solvothermal method, hydrothermal method,

and sol-gel method (Li *et al.*, 2003). Sol-gel processes are widely used for synthesis of transition metal oxides with nanoscaled microstructures. This process provides excellent chemical homogeneity and the possibility of deriving unique metastable structures at low reaction temperatures.

Surface area is one of the important factors for the utilization of titania as catalysts. However, materials with large surface area have high tendency for sintering because of their high surface energies. Thermal stability seriously affects the life of catalyst. Therefore, titania having large surface area with reasonable thermal stability has been sought. Several researchers have attempted to improve thermal stability and activity of titania by adding the second metal oxide to form binary oxide that would be used as photocatalysts. Example of metal oxides includes SiO_2 (Fu *el at*., 1996; Xie *el at.*, 2004), ZrO_2 (Fu *et a*l., 1996; Navio *et al.*, 1997), SnO_2 (Vinodgopal and Kamat, 1995), and CeO_2 (Lin and Yu, 1998). The effects of these second oxides are quite different depending on the procedures of doping and amount of additives. And the mechanisms for stabilization effects of these dopants are not yet fully elucidated.

In this research we focus on the study of effects of calcination conditions on properties and photocatalytic activities of titanium dioxide and mixtures of titanium dioxide and oxides of group IVA and IVB elements. The oxides are prepared by using a sol-gel method and then employed as photocatalysts in photocatalytic oxidation of ethylene in gas phase.

The objectives of this research are as follows:

1. To study the effects of calcination conditions, namely, calcination temperature and time, on crystallite size, phase, and photocatalytic activity of titanium dioxide, which is prepared by a sol-gel method, for photocatalytic oxidation of ethylene.

2. To study the preparation of mixtures of titanium dioxide and oxides of group IVA and IVB elements, using a sol-gel method.

3. To study the effects of type of oxides of group IVA and IVB element added to mixtures of titanium dioxide and oxides of group IVA and IVB elements on photocatalytic oxidation of ethylene.

This thesis is arranged as follows:

Chapter II presents literature reviews of previous works related to this research.

Chapter III explains basic information about titania and other metal oxides such as physical properties and also discusses principles of photocatalytic process.

Chapter IV describes synthesis of various metal oxides employed in this research and experimental apparatus.

Chapter V presents experimental results and discussion.

Chapter VI presents overall conclusions of this research and recommendations for future research.

CHAPTER II

LITERATURE REVIEWS

This chapter is the survey of several studies involving titania and titania-based binary metal oxide photocatalysts. Section 2.1 discusses the use of titanium dioxide as a photocatalyst. Effect of calcination temperature on particle size and photocatalytic activity for pure anatase phase and effect of rutile content on photocatalytic activity are presented. The binary metal oxide for use as photocatalysts, namely, CeO_2-TiO_2, SnO_2-TiO_2, ZrO_2-TiO_2 and SiO_2-TiO_2, are explained in Section 2.2.

2.1 Titanium dioxide for use as photocatalysts

2.1.1 Effect of particle size on photocatalytic activity

Nanocrystalline mesoporous titania was synthesized via a combined sol–gel process with surfactant-assisted templating method (Sreethawong *et al.*, 2005). Titania was heated under various calcination conditions at a temperature between 500^{o}C and 700^{o}C for a duration varying from 1 to 24 hours and was evaluated for its photocatalytic activity through photocatalytic evolution of hydrogen from an aqueous methanol solution. In the synthesis surfactant molecules acted as both mesopore-forming and gelation-assisting agents. The XRD patterns of the samples calcined at 500^{o}C and 600^{o}C showed crystalline structure of pure anatase phase, but partial phase transformation from anatase to rutile was observed at a calcination temperature of 700^{o}C. When both calcination temperature and calcination time increased, crystallinity of titania became greater. When calcination time increased from 1 to 24 hours, BET surface area decreased from 122 to 68 m^2/g, from 70 to 21 m^2/g, and from 29 to 3 m^2/g with calcination temperatures of 500^{o}C, 600^{o}C, and 700^{o}C, respectively. The observed loss in BET surface area was attributable to pore coalescence due to the crystallization of walls separating mesopores.

Subsequently, this tendency caused an increase in mean pore diameter and a decrease in total pore volume of bulk materials.

When considering the photocatalytic activity for hydrogen evolution, the mesoporous TiO_2 treated with optimal thermal treatment conditions of 600°C for 4 hours produced the highest amount of hydrogen. The mesoporous TiO_2 produced significantly higher hydrogen evolution than commercial TiO_2 powders, namely, Ishihara ST-01 and Degussa P-25. Moreover, the photocatalytic activity of titania depended on calcination time. At calcination temperatures of 500°C and 600°C, the maximum amount of hydrogen was observed at calcination times of eight and four hours, respectively. When calcination time increased, the surface area became less while higher crystallinity was observed. The decrease in the photocatalytic activity can be attributed to the decrease in the surface area. The decrease in surface area resulted in fewer number of active surface sites that were accessible to reactant molecules. On the contrary, the hydrogen evolution over titania calcined at 700°C gradually decreased with increasing calcination time. This may be attributed to the decrease in surface area and the presence of a greater extent of rutile phase. In addition, the photocatalytic activity also depended on amorphous phase content of the catalyst. The amorphous phase that was present to some extent in titania calcined at 500°C had a negative effect on the photocatalytic activity of hydrogen evolution because amorphous phase can act as recombination centers for the photogenerated electron-hole pairs.

Jung and coworkers (2004) studied the photoluminescence characteristics of anatase titania particles prepared by the sol–gel method. Using X-ray diffractometry, anatase phase was observed at calcination temperatures between 400°C and 500°C. Rutile phase was detected at the calcination temperature of 600°C. Moreover, the photoluminescence intensity of pure titania particles measured at 77 K gradually increased as the calcination temperature increased. The increase in the photoluminescence intensity indicated that the intersystem crossing of excitons was facilitated while the radiationless decay or the deactivation process for excitons was suppressed. In addition, the photoluminescence was increased due to the reduction of the

internal defects that were responsible for the radiationless recombination of photoexcited electron/hole pairs. The calcination temperature also shifted the maximum peak position of the photoluminescence spectra of titania. A blue shift of the photoluminescence spectrum occurs as a consequence of the enlargement of the band gap of titania as calcination temperature increased. Based on the above results, they concluded that calcination of titania at higher temperature generated more active surface sites that easily reacted with oxygen molecules as well as improved the crystallinity of anatase phase. Consequently, heat treatment of anatase titania particles high temperature gave rise to higher photoactivity as long as no significant rutile phase was formed.

Su and coworkers (2004) investigated the microstructural and chemical properties of TiO_2, obtained by a sol–gel procedure. Titania was prepared by hydrolysis and condensation of titanium (IV) n-butoxide in isopropyl alcohol and was calcined at temperature varying from 400°C to 700^{o}C for two hours. At 400^{o}C, only anatase phase was observed. When calcination temperature was increased to 700^{o}C, the rutile phase became the prevalent phase of TiO_2. The crystal size of TiO_2 increased from 4 to 35 nm as the temperature was increased from 400^{o}C to 700^{o}C while the BET surface area decreased from 122 to11.5 m^2/g.

To examine the photocatalytic activity of titania, the photodecomposition of salicylic acid was carried out. The anatase phase exhibited higher photocatalytic activity than the rutile phase in decomposition of salicylic acid. The changes in the photocatalytic efficiency over the range of calcination temperatures corresponded to the changes in the phase composition of TiO_2. The photocatalytic activity decreased due to the decrease in anatase fraction at the calcination temperatures above 500^{o}C.

Li and coworkers (2003) studied nanocrystalline titania powders synthesized by a sol-gel method. The drying of wet gel was conducted in two ways. Either the gel was dried at 60^{o}C in vacuum, or the material was dried in an evaporator followed by vacuum drying at 80^{o}C. Titania was then calcined at temperatures ranging from 200^{o}C to 1100^{o}C for two hours. At temperature below 800^{o}C, only anatase phase

was observed in the gel dried at 50°C. The transformation from anatase to rutile for the gel dried at 50°C was 200°C higher than that observed for titania gels dried at 60°C. The rutile content increased rapidly until at 1100°C, where all anatase was converted into rutile. One reason for the retardation of the transformation from anatase to rutile in the gel dried at 80°C during sintering was the slower crystal growth of anatase, leading to smaller grain sizes compared to the gel dried at 60°C. Drying conditions may influence the surface/interface of nanoparticles, which in turn affect the nucleation of rutile. To determine the photocatalytic activity of titania powders from gels dried at 80°C, one monitored changes in the absorbance of methylene blue during UV irradiation of up to 30 minutes. The rate at which the intensity of the absorption peak decreased depending on particle sizes of titania. As particle size became smaller, the number of active surface sites increased and so did the surface charge carrier transfer rate in photocatalyst. The volume recombination of charge carriers was also reduced by reduction in particle size. Titania powders with average particles size of 50 nm displayed the highest photocatalytic activity.

Yamazaki and coworkers (2001) studied syntheses of nanocrystalline titania powders using a sol-gel method. Two different acids, namely, sulfuric acid and nitric acid, were used during hydrolysis. Titania was fired at temperatures ranging from100°C to 700°C for four hours. XPS measurements were carried out to determine the elemental components in titania. Titania existed mainly as Ti^{4+} ion and sulfur as SO_4^{2-} ion. More sulfate ions in the prepared solids diffused to the surface by calcination at a temperature between 100°C to 400°C. Similarly, Ward and Ko (1994) reported on zirconia-sulfate cogel prepared by a sol-gel method that crystallization by sintering expelled sulfate ion located in the bulk onto the surface. The sulfate ions on the surface were probably combined with titanium in the bridging bidentate state. On the other hand, the decrease in the sulfate concentration observed at firing temperatures above 400°C was ascribed to the decomposition of sulfate on the surface. For titania prepared with nitric acid, anatase crystals grew continuously with increasing temperatures until they started to convert into rutile at 300°C. This phase transition was almost complete at 500°C. When

calcined at a temperature above 500°C, titania contained large rutile crystals. For titania prepared with sulfuric acid, anatase and rutile phase coexisted at calcination temperatures between 200°C and 500°C as small particles. However, the phase transition from anatase to rutile was complete at 700°C. The incorporation of sulfate ions in the titania prevented crystals from growing and converting to rutile phase. This retardation of crystal growth gave rise to larger specific surface area than those for the pellets prepared with nitric acid. The titania pellets calcined at 200°C by the peptization with nitric acid exhibited maximum activity in the photodegradation of ethylene. Similar experiments were carried out with the titania pellets prepared using sulfuric acid. The degradation rate of ethylene decreased with an increase in firing temperature. For the titania powders prepared with sulfuric acid, the degradation rate was smaller by a factor of three than that for titania prepared with nitric acid. The presence of sulfate ions inhibited the degradation of ethylene, which may be attributed to change in onsets of UV-absorption in titania fired at 200°C and 500°C, or competition between ethylene and sulfate ion for adsorption on the titania surface (Abdullan *et al.*, 1990). With an increase in firing temperature in the range of 200°C to 400°C, the degradation rate increased despite higher concentration of sulfate ion on the surface because of slow growth of titania crystals. However, in the temperature range of 400°C to 500°C, the titania prepared with sulfuric acid exhibited higher catalytic activity than that prepared with nitric acid due to larger specific surface area and the presence of anatase as the predominant form even at high temperatures.

A modified sol-gel process was used to prepare nanostructured titania catalysts of controlled particle size, namely, 6, 11, 16, and 20 nm. (Maira *et al*., 2001). The influence of particle size of titania on photocatalytic oxidation of toluene in the gas phase was investigated under both dry and humid conditions. The conversion increased with decreasing particle size. The increase in conversion was small when the crystal size decreased from 20 to 11 nm, but it is more pronounced for titania of 6 nm size. The higher conversions obtained when particle size decreased from 20 to 16 and 11 nm were mainly due to the increase in specific surface area of titania. Similar trends were observed for photooxidation of trichloroethylene and ethanol in the gas phase over the same series

of titania catalysts. Moreover, as the crystal size of the catalyst increased the production of benzaldehyde as by-product increased. Smaller titania crystals exhibited quantum size effects with a blue shift in the band-gap structure of the catalyst towards higher energies. Fewer photons had sufficient energy to generate the electron-hole pairs needed for the reaction .This led to a decrease in the catalyst activity. The altered band gap structure also modified the redox potential of electron-hole pair and affected the catalyst activity. Beside, having larger specific surface area, smaller catalysts also had different structures from those of bigger crystals. The proportion of corners and edges to planar sites was higher for the catalyst with smaller particle size. Consequently, reactivity and selectivity of the catalyst may be affected. In order to determine the relative contribution of the electronic and structural properties on the catalyst performance, electron paramagnetic resonance spectroscopy (EPR) was used. In the 6 nm titania, holes were trapped by subsurface lattice oxygen forming Ti^{4+}-$[O^{-}]_{lattice}$-Ti^{4+}-OH^{-} species. However, holes were stabilized on the surface to form Ti^{4+}-$[O^{2-}]_{lattice}$-Ti^{4+}-O^{-} species for titania with crystal size larger than 10 nm. Similar observation were reported by Nakaoka and Nosaka (1997). The location of $[O^{-}]_{lattice}$ ion depended on the annealing temperature of titania. Photogenerated holes were stabilized at subsurface location for titania treated at low temperature while high temperature treatment led to coarsening and sintering of titania particles into larger crystal size resulting in trapping of holes at the surface.

2.1.2 Effect of rutile content on photocatalytic activity

Gao and Zhang (2000) studied the effects of amorphous content and particle size on the photocatalytic properties of TiO_2 nanoparticles. Titania nanoparticles were prepared by hydrolysis of $TiCl_4$ followed by calcination at four different temperatures (25°C, 400°C, 600°C and 700°C) for two hours. The activities of ultrafine TiO_2 nanoparticles in the anatase, rutile, or mixed phases were tested in the photocatalytic degradation of phenol. The photocatalytic activity of titania with 42.3% amorphous content is lower than that of titania with 10.5% amorphous content. And the activities of both samples are lower than those of completely crystallized anatase samples despite lower specific surface areas and larger particle sizes. The samples in the rutile

phase contained no amorphous phase. The sample fired at 250°C exhibited higher photocatalytic activity than those fired at 400°C and 600°C because of lower specific surface areas. Titania in the rutile phase showed lower selectivity for mineralization of phenol to CO_2 and H_2O and produced great amount of intermediates such as hydroquinone, catechol, maleic acid, and acetic acid. However, the photocatalytic activity of rutile was comparable to that of anatase.

2.2 Binary metal oxide for use as photocatalysts

Binary metal oxides can be used as photocatalysts. Most photocatalysts are combinations of titanium dioxide and another metal oxide. Four such combinations, namely, SiO_2-TiO_2, ZrO_2-TiO_2, SnO_2-TiO_2, CeO_2-TiO_2, are discussed here.

2.2.1 SiO_2-TiO_2

Nanocrystalline silica-embedded titania powder was prepared by hydrolysis under ultrasonic irradiation (Liu *et al.*, 2004). The ratio of silicon to titanium in the sample was in the range of 0 to 20%. Crystallite size decreased sharply with increasing silica content up to 10%. When the silica content exceeded 10%, there was no significant change in the crystallite size of silica/titania particles with changing the silica content. When titania was embedded with silica, crystallite growth was suppressed and specific surface area remained large. Moreover, specific surface area was increased with increasing the silicon content. Suitable addition of silica into titania matrix helped to suppress the reduction of surface area at high calcination temperature. The photocatalytic activity of silica/titania powders for decomposition of formaldehyde was increased with increasing silica content up to 10%. The highest photocatalytic activity was obtained for titania containing 10% silica. Embedding silica into anatase titania matrix improved the photocatalytic activity for decomposition of formaldehyde as a result of larger specific surface area and hydroxyl group content.

Xie and coworkers (2004) investigated photocatalytic activity of titania–silica mixed oxides. The content of SiO_2 was in the range from 4.7 to 50 % and the

samples were calcined at temperatures ranging between 400°C and 800°C for two hours. Crystallite size of mixed oxide was significantly decreased as a small amount of silica was added with respect to pure TiO_2 calcined at same temperature. Moreover, the crystallite size was further decreased with more silica added. Therefore, the addition of silica inhibited the growth of titania crystals and suppressed the phase transformation from anatase to rutile. From FT-IR spectra, the band at 948 cm^{-1} was associated with the Ti–O–Si linkages, which indicated the interaction between titania and silica at molecular-scale that enhanced surface properties and photocatalytic activity. The peaks at 1623 and 3434 cm^{-1} assigned to the stretching vibration of OH group and molecular H_2O were obviously removed as the calcination temperature raised up. The surface of mixed oxide became clean and the density of surface bulk defects was reduced with increasing the calcination temperature. In case of photocatalytic activities of titania–silica mixed oxide, the activities of mixed oxides (Si ≤16.6 mol%) was much higher than that of pure TiO_2 and the maximum activity occurred at SiO_2 content of 9.1%. The enhanced photocatalytic activity of titania–silica mixed oxide was ascribed to the three reasons. Firstly, anatase phase of titania was formed at higher temperature (600°C) when silica was added into titania. Photocatalytic activity of anatase phase was believed to be superior to rutile phase. Secondly, crystallite size of mixed oxide was smaller than that of pure TiO_2 calcined at same temperature. Finally, Brønsted acidity is generated when a suitable amount of silica is added. Brønsted acidity increased content of surface hydroxyl groups, which accepted photoinduced holes to form OH radicals and then oxidized adsorbed organic molecules. When 50 mol% silica was added into mixed oxides, activity of catalyst drastically dropped because the transformation from amorphous to anatase was inhibited and surface active sites were covered by excessive inactive silica.

Silica/titania and zirconia/titania mixed oxides were prepared by a sol–gel technique, using titanium ethoxide, tetraethylorthosilicate, and zirconium(IV) propoxide as precursors of titania, silica, and zirconia, respectively (Jung *et al.*, 2004). Silica/titania mixed oxides were calcined at temperatures between 400°C and 800°C, and the content of silicon was varied from 0% to 60%. The content of zirconium in zirconia/titania mixed

oxide was varied from 0% to 20%. Photocatalytic decomposition of trichloroethylene was employed to determine activities of mixed oxides. Silica/titania mixed oxides contained only anatase phase and no rutile phase. At a fixed content of silica, the photoactivity increases monotonically with increasing crystallite size. When silica content is less than 10%, increase of specific surface area was not substantial because increase of calcination temperature easily induced grain growth of anatase phase as in pure titania. On the other hand, grain growth was inhibited when silica content exceeded 10%. As a result, larger surface area could be obtained in the samples. In addition, quantization of band structure was observed when silica content excessed 10%. This quantized band structure confined photoexcited electrons within conduction band and retarded recombination of charge carriers. Consequently, photoactivity should improved. When the content of silica was over 10%, the quantization of band structure caused photoactivity of silica/titania particles to be more sensitive to the change in crystallite size. For zirconia/titania mixed oxides, addition of zirconia beyond 10% was effective to enhance the thermal stability of titania for the phase transition. Unlike silica/titania mixed oxide, the photoactivity of zirconia/titania mixed oxides at all compositions was not higher than that of pure titania. The photoactivity monotonically decreased as the content of zirconia increased although no rutile phase was formed even at a calcination temperature of 700^{o}C when zirconia content was greater than 10%. The photoactivity linearly increased with the crystallite size. From this result, the photoactivity of titania-based photocatalyst was believed to linearly depend on the crystallite size of anatase phase.

Another silica-doped nanocrystalline titania powders were prepared by a sol-gel process (Cheng *et al*., 2003). The samples were calcined at the temperatures ranging from 400°C to 950^{o}C for two hours. It was found that optimum amount of silica could effectively suppress phase transformation of titania from anatase to rutile and could prevent growth of titania crystal. But excessive silica could not prevent the phase transformation because of phase separation between titania and silica. At the optimal silica content of 30 wt%, doped titania powders displayed high photoactivities and inhibiting effect on the phase transformation. In addition, presence of Ti^{3+}, as detected by

EPR and XPS, proved the occurrence of deoxidization in silica/titania samples after heat treatment and the existence of oxygen vacancies in the nanoparticles. All these effects contributed to the higher photoactivity of silica-doped titania powders.

Hong and coworkers (2003) studied pure TiO_2 and TiO_2-SiO_2 nanoparticles. From thermal analysis and XRD analysis, rutile phase was detected in pure titania when calcination temperature was above 700^oC. No rutile was observed for the TiO_2-SiO_2 particles for calcination temperature up to 800^oC. Crystallite size of prepared particles decreased and specific surface area monotonically increased with increasing silica content. The photocatalytic activities of pure TiO_2 and TiO_2/SiO_2 particles were determined using decomposition of *p*-nitrophonol. The photocatalytic activity of mixed oxide increased with an increase in silica content up to 10% and was higher than that obtained from pure TiO_2 particles. However, photocatalytic activity of mixed oxide decreased when silica content exceeded 10%. In addition, pore volume and pore size of TiO_2-SiO_2 particles reached maximum values at 10 wt.% silica in titania. Therefore, large pore volume and pore size facilitated mass transfer of reactants. The increase in specific surface area by the formation of small pores was not always effective for high photocatalytic activity and the optimum composition of silica to titania was 10%.

2.2.2 ZrO_2-TiO_2

The influences of doping ZrO_2 into the anatase TiO_2 on the photocatalytic activity and phase stability of directly formed nanometer-sized particles were investigated by Hirano and coworkers (2003). Anatase TiO_2 doped with 4.7 and 12.4 mol% ZrO_2, which were synthesized by simultaneous hydrolysis under hydrothermal conditions at 200°C, displayed higher photocatalytic activity than pure anatase TiO_2 for decomposition of methylene blue. The enhancement in photocatalytic activity of the ZrO_2-doped TiO_2 might be explained by the increase in concentration of oxygen vacancies in the structure creating solid solutions by substituting Zr ions for Ti ions might produce structural defects such as vacancies in the lattice, particularly on the surface to partially offset the lattice strain. Therefore, oxygen could escape from the surface of the lattice to trap

photogenerated holes. Crystal growth and phase transformation from anatase to rutile brought about by heating at high temperature were retarded by doping ZrO_2 into TiO_2. Anatase TiO_2 doped with ZrO_2 exhibited high thermal stability against phase transformation and maintained anatase structure even after being fired at 1000°C for one hour.

2.2.3 SnO_2-TiO_2

Particulate film of TiO_2 and SnO_2 was prepared from a mixture of TiO_2 and SnO_2 colloidal suspensions (Vinodgopal and Kamat, 1995). By employing a coupled SnO_2-TiO_2 semiconductor system, the rate of electrochemically assisted photocatalytic degradation of the dye in aqueous solution was enhanced. The improved charge separation as a result of coupling two semiconductor systems with different energy levels and the applied anodic bias responsible for the enhancement in the rate of photocatalytic degradation. Moreover, nanostructured semiconductor films of SnO_2, TiO_2 and SnO_2-TiO_2 were employed for electrochemically assisted photocatalytic degradation of a textile azo dye naphthol blue black (NBB) (Vinodgopal *et al.*, 1996). The degradation rate was significantly higher for SnO_2-TiO_2 composite films than SnO_2 and TiO_2 films alone. The enhanced degradation rate of NBB using composite semiconductor films was attributed to increased charge separation in these systems. Substitution of tin for titanium in rutile TiO_2 increased the photoactivity of the rutile by up to 15 times for the oxidation of acetone (Lin *et al*., 1999). The activity increased with increasing tin content, and reached maximum vale at a tin content of 0.075. Poor photocatalytic activity of pure rutile was a result of fast electron–hole recombination in rutile TiO_2, not lack of hydroxyl groups on its surface. Addition of tin to rutile TiO_2 lattice can effectively slow down the recombination rate.

2.2.4 CeO_2-TiO_2

The photocatalytic activities of the mixtures of TiO_2 (P25) with three rare earth oxides namely, Y_2O_3, La_2O_3, and CeO_2, (Lin and Yu, 1998) were investigated.

Effects of the rare earth oxide contents and calcination temperature on the photocatalytic activities were studied. Mixtures of TiO_2 with La_2O_3 (0.5 wt.%) or Y_2O_3 (0.5 wt. %) that were calcined at 700°C or 650°C exhibited higher photoactivities than pure TiO_2 for the oxidation of acetone. On the other hand, mixtures of TiO_2 with CeO_2 have lower photoactivity than pure TiO_2. Experimental results of polycrystalline X-ray diffraction, photoexcited transient absorption decay and zeta potential measurements showed that the presence of these rare earth oxides inhibited transformation from anatase to rutile at elevated temperatures. The lower photocatalytic activity of TiO_2-CeO_2 mixtures was due to fast recombination rate of photogenerated electron-hole pairs and high isoelectric point in terms of pH value. Lower isoelectric point lead to more hydroxide ions on the surface of catalyst. Consequently, hydroxide ions acting as hole traps that prevented electron-hole recombination and gave rise to high photoactivity.

Sinha and Suzuki (2005) studied mesoporous ceria-titania with different Ce/Ti ratios (0.5:1, 1:1, 1:1.5). The mixed oxides had large specific surface areas with narrow pore size distributions in the mesoporous range after calcination at 700°C. The material showed high activities for removal of ethylene at room temperature, compared to nonporous ceria-titania, mesoporous ceria, and mesoporous titania.

CHAPTER III

THEORY

This chapter consists of three main sections. Section 3.1 discusses properties and applications of materials used in the research. Synthesis of such materials by sol-gel method is described in Section 3.2. Details of photocatalytic processes are discussed in Section 3.3.

3.1 Materials used as photocatalysts.

This section discusses properties and applications various metal oxides, namely, titanium dioxide, silicon dioxide, zirconium dioxide, tin dioxide, and cerium dioxide. These materials were used as catalysts for photocatalytic oxidation of organic compounds in gas phase.

3.1.1 Titanium dioxide

3.1.1.1 Physical and Chemical Properties (Othmer, 1991; Fujishima *et al.*, 1999)

Titanium dioxide may take on any of the following three crystal structures: anatase, which tends to be more stable at low temperature; brookite, which is usually found only in minerals; and rutile, which tends to be more stable at higher temperatures and thus is sometimes found in igneous rock.

Anatase generally shows a higher photocatalytic activity than the other types of titanium dioxide. Comparison of same physical properties of rutile and anatase is shown in Table 3.1.

Table 3.1 Comparison of rutile, brookite and anatase. (Othmer, 1991 and Fujishima *et al.*, 1999).

Properties	Anatase	Brookite	Rutile
Crystal structure	Tetragonal	Orthorhombic	Tetragonal
Optical	Uniaxial, negative	Biaxial, positive	Uniaxial, negative
Density, g/cm^3	3.9	4.0	4.23
Harness, Mohs scale	$5^1/_2 - 6$	$5^1/_2 - 6$	$7 - 7^1/_2$
Unit cell	$D_4a^{19}.4TiO_2$	$D_2h^{15}.8TiO_2$	$D_4h^{12}.3TiO_2$
Dimension, nm			
a	0.3758	0.9166	0.4584
b	-	0.5436	-
c	0.9514	0.5135	2.953
Refractive index	2.52	-	2.52
Permittivity	31	-	114
Melting point	changes to rutile at high temperature	-	1858˚C

The reason that anatase is more photoactive than rutile may lie in the differences in their so-called energy band structures. The band gap energy of a semiconductor is the minimum energy of light required to make the material electrically conductive or, in other words, to get the electrons excited enough to get moving. The band gap energy of anatase is 3.2 eV, which corresponds to UV light with wavelength of 388 nanometers, while the band gap energy for the rutile type is 3.0 eV, corresponding to violet light that has a wavelength of 413 nanometers. The level of the conduction band for anatase is 0.2 eV higher than that for rutile. In more technical terminology, the band

gap energy for a semiconductor indicates the minimum energy of light necessary to produce electrons in the conduction band (CB) and give rise to electrical conductivity (photoconductivity) and “holes,” which are actually the absence of electrons, in the valence band (VB). These holes can react with water to produce the highly reactive hydroxyl radical (•OH). Both holes and hydroxyl radicals can oxidize most organic materials.

The VB energies for both anatase and rutile are very low in the energy. Consequently, the VB holes (and the hydroxyl radicals) have great oxidizing power. The CB energy for rutile is close to the potential required to electrolytically reduce water to hydrogen gas, but that for anatase is higher in the energy, meaning that it has higher reducing power. Therefore, anatase can drive the very important reaction involving the electrolytic reduction of molecular oxygen (O_2) to superoxide ($O_2\bullet^-$).

Although anatase and rutile are both tetragonal, they don't have the same crystal structures. Anatase exists in near-regular octahedral and rutile forms slender prismatic crystal. Rutile is the thermally stable form and is one of the two most important ores of titanium.

The three forms of titanium (IV) oxide have been prepared in laboratories but only rutile, the thermally stable form, has been obtained in the form of transparent large single crystal. The transformation from anatase to rutile is accompanied by the evolution of ca. 12.6 kJ/mol (3.01 kcal/mol), but the rate of transformation is greatly affected by temperature and by the presence of other substance which may either catalyze or inhibit the reaction. The lowest temperature at which conversion of anatase to rutile takes place at a measurable rate is around 700˚C, but this is not a transition temperature. The change is not reversible since ΔG for the change from anatase to rutile is always negative.

Brookite has been produced by heating amorphous titanium (IV) oxide, which is prepared from an alkyl titanate or sodium titanate, with sodium or potassium hydroxide in an autoclave at 200 to 600°C for several days. The important commercial forms of titanium (IV) oxide are anatase and rutile, and they can readily be distinguished by X-ray diffraction spectrometry.

Since both anatase and rutile are tetragonal, they are both anisotropic, and their physical properties, e.g. refractive index, vary according to the direction relative to the crystal axes. In most applications of these substances, the distinction between crystallographic direction is lost because of the random orientation of large numbers of small particles, and only average values of the properties are significant.

Measurement of physical properties, in which the crystallographic directions are taken into account, may be made for both natural and synthetic rutile, natural anatase crystals, and natural brookite crystals. Measurements of the refractive index of titanium (IV) oxide must be made by using a crystal that is suitably orientated with respect to the crystallographic axis as a prism in a spectrometer. Crystals of suitable size of all three modifications occur naturally and have been studied. However, rutile is the only form that can be obtained in large artificial crystals from melts. The refractive index of rutile is 2.75. The dielectric constant of rutile varies with direction in the crystal and with any variation from the stoichiometric formula, TiO_2; an average value for rutile in powder from is 114. The dielectric constant of anatase powder is 48.

Titanium (IV) oxide is thermally stable (mp 1855 °C) and very resistant to chemical attack. When it is heated strongly under vacuum, there is a slight loss of oxygen corresponding to a change in composition to $TiO_{1.97}$. The product is dark blue but reverts to the original white color when it is heated in air. Hydrogen and carbon monoxide reduce it only partially at high temperatures, yielding lower oxides or mixtures of carbide and lower oxides. At ca. 2000 ˚C and under vacuum, carbon reduces it to titanium carbide. Reduction by metal, e.g., Na, K, Ca, and Mg, is not complete.

Chlorination is only possible if a reducing agent is present; the position of equilibrium in the system is

$$TiO_2 + 2Cl_2 \rightarrow TiCl_4 + O_2$$

3.1.1.2 Applications of titanium dioxide

Titanium dioxide is one of the most basic materials in our daily life. Titanium dioxide has been widely used in a variety of paints, plastics, paper, inks, fibers, cosmetics, sunscreens and foodstuffs.

Naturally, the type of titanium dioxide that is used as a pigment is different from that used as a photocatalyst. The photocatalytic technology is becoming more and more attractive to industries today because environmental pollution has been recognized as a serious problem that needs to be addressed immediately. Various applications in which research and development activities involving titanium dioxide have been investigated, such as fog-proof, anti-bacterial, anti-viral, fungicidal, anti-soiling, self-cleaning, deodorizing, air purification, anti-cancer, water treatment and water purification.

3.1.2 Silicon dioxide

3.1.2.1 Physical and Chemical Properties

Silicon dioxide occurs naturally as sand or rock and when melted, the resulting product is called fused quartz. Today, nanocomposites of silicon dioxide are prepared by sol-gel method. Moreover, silicon dioxide is generally amorphous. Then silicon dioxide alone is impractical as a catalyst because of its low catalytic activity (Yang *et al.*, 2003).

3.1.2.2 Applications

The applications of silicon dioxide include matting agent for paint (wood/industrial/PCM) and ink, anti-blocking agent for plastic film (PP, PE, PET etc.),

printability improving agent for inkjet paper, film or textile, antifoaming aids, anti-caking agent for deliquescent powder, stabilizer for beer, abrasive for transparent toothpaste, solid carrier, absorbent, abrasive and catalyst support.

3.1.3 Zirconium dioxide

3.1.3.1 Physical and Chemical Properties

Zirconium dioxide or zirconia (ZrO_2) as a pure oxide does not occur in nature; but it is found in baddeleyite and zircon ($ZrSiO_4$) which form the main sources for the material. Of the two of these, zircon is by far the most widespread, but it is less pure and requires a significant amount of processing to yield zirconia. The processing of zirconia involves the separation and removal of undesirable materials and impurities, silica, in the case of zircon and iron and titanium oxides for baddeleyite. There are several routes to the extraction of zirconia from zircon including chlorination, alkali oxide decomposition, lime fusion and plasma dissociation.

Pure zirconia exists in the monoclinic form at room temperature. Cubic and tetragonal phases are stable at higher temperatures. The transformation of monoclinic to cubic zirconia occurs at a temperature between 800 and1000°C, and accompanied by a large change in lattice size. A consequence of this phase change is a large volume expansion on cooling which make the fabrication of pure zirconia ceramics impossible.

3.1.3.2 Applications

Zirconia is an important material widely used in ceramics technology and in heterogeneous catalysis. Due to its nature as n-type semiconductor, it has been considered recently as a photocatalyst in photochemical heterogeneous reactions. Moreover, the reported values of the energy of the band gap energy (E_g) of this oxide range between 3.25 and 5.1 eV, depending on the preparation technique of the

sample. From these, the most frequent and accepted value is 5.0 eV (Botta *et al.*,1999). In addition, zirconia is also used in composite cutting tools and abrasive wheels. Moreover, zirconia are used such as seals, valves and pump impellers and used as a femoral head component in hip implants and so on.

3.1.4 Cerium dioxide

3.1.4.1 Physical and Chemical Properties

The band gap energy of cerium dioxide or ceria (CeO_2) with the cerianite structure is 3.1 eV, being able to filter out UV rays less than 400 nm in wavelength (Sato *et al.*, 2004). Moreover, CeO_2 is abundant, nontoxic and inexpensive.

3.1.4.2 Applications

CeO_2 is widely employed as sun care products and the most used oxygen storing component in automotive three-way catalysts. And ceria is frequently used in combination with other oxides. Nowadays, CeO_2 can be used as a material for photocatalyst in the photooxidation of water and other VOCs (Bamwenda and Arakawa, 2000).

3.1.5 Tin dioxide

3.1.5.1 Physical and Chemical Properties

Tin dioxide (SnO_2) with the rutile structure is a wide energy band gap ~3.8 eV n-type semiconductor (Vinodgopal and Kamat, 1995). In particular, SnO_2 thin films have drawn much interest because of their potential application in microsensor devices. Taking into account its potential application and the importance for fundamental research as well as its simple structure, SnO_2 is an ideal model system for a systematic investigation on microstructure, grain boundary and interface characteristics, and their effects on physical properties.

3.1.5.2 Applications

Tin dioxide is used as an oxidation catalyst (Lin *et al.*, 1999), gas sensor material, thin film micro-battery and transparent electrodes for flat panel displays and solar cells.

3.2 Sol-gel method (Fu *et al.*, 1996; Su *et al.*, 2004)

This process occurs in liquid solution of organometallic precursors such as tetraethyl orthosilicate, zirconium propoxide and titanium isopropoxide, which, by means of hydrolysis and condensation reaction, lead to the formation of sol.

$$M\text{-}O\text{-}R + H_2O \Rightarrow M\text{-}OH + R\text{-}OH \quad \text{(hydrolysis)} \quad (3.1)$$

$$M\text{-}O\text{-}H + HO\text{-}M \Rightarrow M\text{-}O\text{-}M + H_2O \quad \text{(water condensation)} \quad (3.2)$$

$$M\text{-}O\text{-}R + HO\text{-}M \Rightarrow M\text{-}O\text{-}M + R\text{-}OH \quad \text{(alcoholcondensation)} \quad (3.3)$$

A typical example of a sol-gel method is the addition of metal alkoxides to water. The alkoxides are hydrolyzed giving the oxide as a colloidal product.

The sol is made of solid particles of a diameter of few hundred nanometers suspending in a liquid phase. After that, the particles condense into gel, in which solid macromolecules are immersed in a liquid phase. Drying the gel at low temperature (25-100˚C), produces porous solid matrices or xerogels. To obtain a final product, the gel is heated. This heat treatment serves several purposes, *i.e.*, to remove solvent, to decompose anions such as alkoxides or carbonates to give oxides, to rearrange of the structure of the solid, and to allow crystallization to occur.

Using the sol-gel method, one can easily control a stoichiometry of solid solution and a homogeneous distribution of nanoparticles and metal oxides. In addition, the advantages are that the metal oxides are prepared easily at room temperature and high purity can be obtained.

3.3 Theory of photocatalytic oxidation

The primary photocatalytic process occurs upon irradiation of a semiconductor. A semiconductor is characterized by an electronic band structure, in which the highest occupied energy band, or valence band, and the lower empty band, conduction band, are separated by a band gap. The magnitude of the energy of band gap between the electronically populated valence band and the largely vacant conduction band governs the extent of thermal population of the conduction band in its intrinsic state. The band gap defines the wavelength sensitivity of the semiconductor to irradiation (Fox and Dulay, 1993). A photon of energy higher than or equal to the band gap energy is absorbed by a semiconductor particle. Then an electron from the valence band is promoted to the conduction band with simultaneous generation of an electronic vacancy or "hole" (h^+) in the valence band. This process is photoexcitation of electrons. Figure 3.1 shows the photocatalytic process occurring on an irradiated semiconductor particle.

In most materials that are electrically conductive, i.e., metals, two types of charge carriers, electrons (e^-) and holes (h^+), immediately recombine on the surface or the bulk of particle in a few nanoseconds and the accompanying energy is dissipated as heat (see Equation 3.4). On semiconductor such as titanium dioxide, however, they survive for longer periods of time to allow these carriers can be trapped in surface states where they can react with donor (D) or acceptor (A) species adsorbed or close to the surface of the particle (Equations 3.5, 3.6, and 3.7) (Litter, 1999). Subsequently, oxidation and reduction can be initiated.

Recombination $$h^+ + e^- \rightarrow heat \quad (3.4)$$

Photoexcitation $$Semiconductor + h\nu \rightarrow e^- + h^+ \quad (3.5)$$

$$h^+ + D \rightarrow D^+ \quad (3.6)$$

$$e^- + A \rightarrow A^- \quad (3.7)$$

Electron-hole recombination processes may be suppressed by bulk and surface traps. In Figure 3.2, the energy levels of the bulk and surface traps fall within the band gap. The surface and bulk traps are localized, and the electrons trapped in such states are thus associated with a particular site on the surface or in the bulk of the solid. The population of bulk and surface traps depend on two factors, namely, the decrease in entropy that occurs

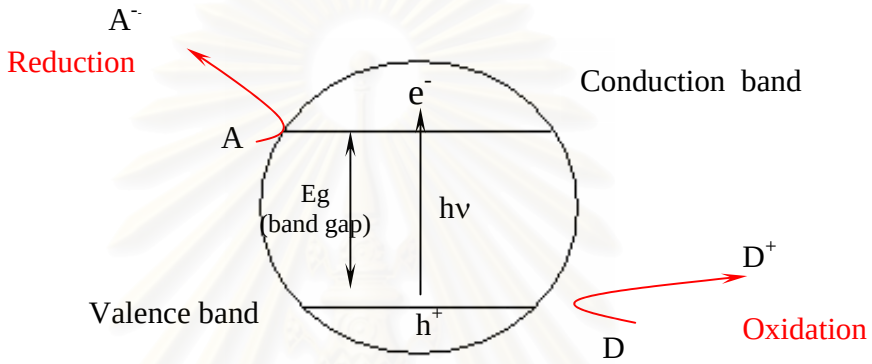

Figure 3.1 Photocatalytic process occurring on an illuminated semiconductor particle (Litter, 1999).

when electrons are trapped, and the difference in relative energy between the traps and the bottom of the conduction band.

In aqueous solution, hydroxyl radicals ($^{\bullet}OH$) production is favorable because of the abundance of hydroxyl groups and water molecules on the surface of catalyst. However, in the gas phase, organic substrates can themselves act as adsorbed traps for the photogenerated hole since in the gas phase, water molecules are not the predominant species in contact with the catalyst. Although in the presence of water vapor, OH groups are presented on the catalyst surface and their contribution to photooxidation can not be discarded (Alherici *et al.*, 1997).

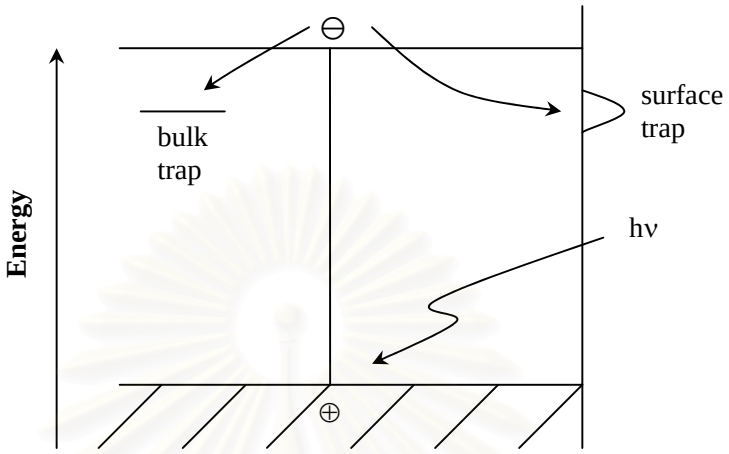

Figure 3.2 Surface and bulk electron trapping (Linsebigler *et al.*, 1995).

When adsorbed water molecules are oxidized by holes, hydroxyl radicals, which have strong oxidizing power, are formed (Equations 3.8 and 3.9).

$$h^+ + H_2O \rightarrow {}^{\bullet}OH + H^+ \qquad (3.8)$$

$$h^+ + OH^- \rightarrow {}^{\bullet}OH \qquad (3.9)$$

The hydroxyl radicals can then react with organic components, initially producing free radicals. When molecular oxygen is present (reactions always occur in the presence of oxygen from the air in the use of the photocatalyst for environment), It can react with these free radicals producing organic peroxyl radicals. These radicals can then take part in chain reactions. In a short time, organic compounds are completely degraded, i.e., converted into carbon dioxide and water.

Meanwhile, the electrons that are produced in the electron-hole pairs are also put to work. These electrons are used to reduce (i.e., add electrons) to oxygen in air. Because oxygen is easier to reduce than water, it will tend to be reduced, producing the superoxide radical anion (O_2^-) Equation 3.10

$$e^- + O_2 \rightarrow O_2^- \qquad (3.10)$$

The superoxide anion attaches itself to the peroxyl radicals mentioned above. The resulting unstable product now contains at least four oxygens and can decompose to produce a carbon dioxide molecule. On the molecular scale, superoxide acts like a "supercharge ", greatly increasing the oxidation process, which is in fact a form of combustion. In addition to this mechanism, another interpretation proposed recently is that the formation of atomic oxygen ($O^{\bullet}$), which is extremely reactive in air, leads to a direct attack on the carbon bonds in organic material.

In Figure3.3, in terms of energy usage, the complete electrolytic decomposition of water is possible if the energy of the conduction band is at least as negative (i.e., higher in the diagram) as that required to reduce water to oxygen gas (0.0 V in acid solution), and the VB is at least as positive (i.e., lower) as that required to oxidize water to oxygen gas (+1.23 V). The complete decomposition of water is thus theoretically possible if a semiconductor that has the minimum band gap energy of 1.23 eV is illuminated with light, assuming that the energies of valence band and conduction band are located at appropriate positions. All of the semiconductors with small band gaps, however, have a strong tendency to decompose and dissolve when illuminated in aqueous solution.

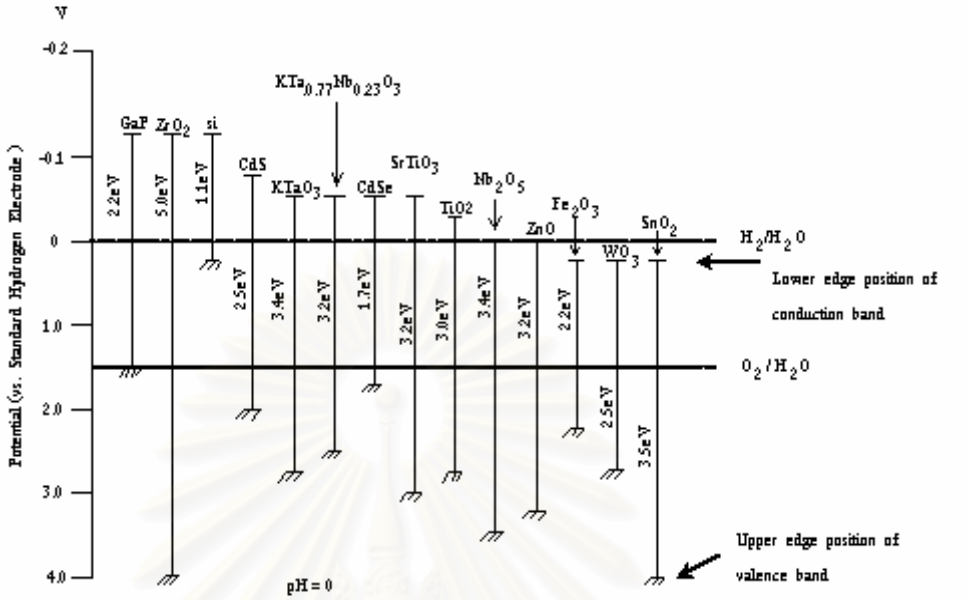

Figure 3.3 Energy diagram for typical semiconductors. (Fujishima *et al.*, 1999)

CHAPTER IV

MATERIALS AND METHODS

This chapter discusses various materials and methods employed in this research. The chapter is divided into three parts including catalyst preparation, catalyst characterization and in photocatalytic activity measurement.

Section 4.1 describes preparation of various metal oxides to be used as photocatalysts. Section 4.2 discusses several characterization techniques for catalysts, including of X-ray fluorescence spectroscopy, X-ray diffractometry, Nitrogen adsorption, Electron spin resonance spectroscopy and Infrared Spectroscopy. Finally, the experimental apparatus and procedures used in evaluating the performance of the photocatalysts are explained in Section 4.3.

4.1 Preparation of catalysts

This section describes methods for preparation of various metal oxides to be employed as photocatalysts using sol-gel processes.

4.1.1 Preparation of titanium dioxide

Titanium dioxide was prepared using a sol-gel method, and titanium isopropoxide (Aldrich Chemical, Milwaukee, WI) was employed as a precursor. First, 7.33 ml of 70% nitric acid (Asia Pacific Specialty Chemicals Limited) was added to 1000 ml of distilled water. While the acidic solution was stirred, 83.5 ml of titanium isopropoxide was added slowly. The suspensions were stirred continuously at room temperature for about 3 days until clear sol was obtained. After that, the sol was dialyzed in a cellulose membrane with a molecular weight cutoff of 3500 (Spectrum Companies, Gardena, CA). Prior to use, the dialysis tubing was washed in an aqueous solution of

0.001M EDTA and 2% sodium hydrogen carbonate. The wash solution was prepared by dissolving 0.372 grams of EDTA (Asia Pacific Specialty Chemicals Limited) and 43 grams of sodium hydrogen carbonate powder, 99.93% (Fisher Scientific Chemical) in one liter of distilled water. Dialysis tubing was cut into sections of 32 cm in length and was submerged in the wash solution. Then the membrane was heated to 80 °C and held there for 30 minutes while simultaneously being stirred. After the solution was cooled to room temperature, the tubing was again washed with distilled water. The tubing was again immersed in one liter of fresh distilled water while being stirred continuously, and was heated to 80°C. The tubing was rinsed one more time and was stored in distilled water at 4°C until needed. The clear sol was placed in dialysis tubing. Then the tubing containing the sol was submerged in distilled water using a ratio of 100 ml of sol per 700 ml of distilled water. The water was changed daily for 3-4 days until the pH of the water reached 3.5. To remove solvents, the dialyzed sol was left in ambient atmosphere overnight and was dried at 110°C. The resulting gel was then ground. Finally, titania nanoparticles were fired at desired temperature, namely, 200°C, 320°C, 350°C or 380°C, for the duration of 1 to 3 hours.

4.1.2 Preparation of titania-zirconia mixed oxides

To obtain a sol containing both titania and zirconia, individual sols containing each oxide must first be prepared separately and later mixed. For zirconia sol, we prepared an acidic solution by mixing 1.1 ml of nitric acid with 52.6 ml of distilled water. The solution was stirred while 3.8 ml of zirconium propoxide was added. A white precipitate immediately formed to bring about a cloudy suspension during the addition. The suspension was then stirred continuously for 3-4 days to obtain the clear sol.

A titania sol was prepared using the same procedure described in Section 4.1.1. However, different amounts of starting materials were used in this case. The amounts of nitric acid, distilled water, and titanium isopropoxide needed are 3 ml, 409.2 ml and 34.2 ml, respectively.

After the two sols were mixed by stirring about 30 minutes, the mixture was placed in dialysis tubing (Spectra Por with a molecular weight cutoff value of 3500). And the sol was dialyzed against distilled water for 3-4 days until the pH of the water reached 3.5. To remove solvents, the dialyzed sol, the sol was left in ambient atmosphere overnight and was dried at 110°C. The resulting gel was then ground. Finally, titania–zirconia nanoparticles were fired at 200°C for one hour.

4.1.3 Preparation of titania-silica mixed oxides

To prepare a mixture containing both titania and silica, a sol of tiania and silica needed to be prepared separately. To prepare the silica sol, one mixed 6.6 ml of tetraethyl orthosilicate with 2.1 ml of distilled water, 1.7 ml of ethanol, and 0.2 ml of hydrochloric acid. The mixture was stirred for 30 minutes, then clear silica sol was obtained.

Titania sol was prepared by mixing 2.5 ml of nitric acid with 341 ml of distilled water. The solution was stirred while 28.5 ml of titanium isopropoxide was added. White precipitate immediately formed to produce a cloudy suspension during the addition. Then the suspension was stirred continuously for 3-4 days to obtain the clear sol.

After sols of titania and silica were mixed by stirring about 30 minutes, the mixture was placed in dialysis tubing (Spectra Por with a molecular weight cutoff value of 3500). The sol was dialyzed against distilled water for 3-4 days until the pH of the water reached 3.5. To remove solvents from the dialyzed sol, the sol was left in ambient atmosphere overnight and was dried at 110°C. The resulting gel was ground and was fired at 200°C for one hour.

4.1.4 Preparation of titania-ceria mixed oxides

To obtain a sol containing both titaina and ceria, individual sol containing each oxide must first be prepared separately and was later mixed. Ceria sol was prepared

by mixing 0.78 grams of cerium (III) nitrate hexahydrate with 10.7 ml of distilled water. The solution was stirred while 21.6 ml of 20 vol% ammonium hydroxide was added until pH of the solution reached 10. Precipitation occurred and precipitate was stabilized by adding 4.5 ml of nitric acid until pH of solution reached 3.3. The suspension is then stirred continuously overnight. Titania sol was prepared in the same manner described in Section 4.1.2. Then sols of titania and ceria were mixed and the mixture was dialyzed in the same manner described in Section 4.1.2.

To obtain powder, the dialyzed sol was left in ambient atmosphere overnight and was dried at 110°C. The resulting gel was ground and was fired at 200°C for one hour.

4.1.5 Preparation of titania-tin dioxide mixed oxide

To prepare the tin dioxide sol, one mixed 2.7 grams of tin (II) chloride dihydrate with 59.8 ml of distilled water under constant stirring and heating at 70°C. After that, 17.9 ml of tartaric acid was added to the solution. Later, 37.9 ml of 2M NH_4OH solution was added to bring about precipitation of organometallic compound. This precipitation occurred at a pH between 2 and 3. The precipitate was separated using a centrifuge at 3,000 rpm for 20 minutes and was then washed with ethanol five times. The resulting paste, tin (II) tartarate, was employed as a starting material for the preparation of tin dioxide sol. 60 ml of ethanol and 60 ml of distilled water were added to tin (II) tartarate paste, while being stirred. Finally, 0.2 ml of HNO_3 was added to bring about pH value of 2.9. Titania sol was prepared in the same manner described in Section 4.1.2. Then sols of titania and tin dioxide were mixed and the mixture was dialyzed in the same manner described in Section 4.1.2.

To obtain powder, the dialyzed sol was left in ambient atmosphere overnight and was dried at 110°C. The resulting gel was ground and was fired at 200°C for one hour.

4.2 Characterization of catalysts

In order to determine physical and chemical properties of catalysts, various characterization techniques were employed. Such techniques are discussed in this section.

4.2.1 X-ray fluorescent spectroscopy (XRF)

XRF was used to determine composition in the bulk of catalysts. The analysis was performed using Philips: PW 2400 at the Scientific and Technological Research Equipment Center, Chulalongkorn University (STREC).

4.2.2 X-ray diffractomety (XRD)

XRD was employed to identify crystal phase, crystallinity, and crystallite size of metal oxide. The equipment used was a SIEMENS D 5000 X-ray diffractometer with CuK_{α} radiation with Ni filter in the 2θ range of 20-60° with a resolution of 0.04^{o}.

4.2.3 Nitrogen adsorption

Nitrogen adsorption isotherms were determined at liquid nitrogen temperature of 77K. Brunauer-Emmett-Teller (BET) approach was utilized to determine specific surface area. And Barrett-Joyner-Halenda (BJH) approach was employed for calculation of mean pore size and pore size distribution. The equipment used was at Department of Chemical Engineering, Faculty of Engineering, Burapa University.

4.2.4 Electron spin resonance spectroscopy (ESR)

ESR measurements were carried out at 77 K with a JES-RE2X ESR spectrometer. Recorded spectra were scanned and were converted to a g value scale

referring to a Mn^{2+} marker at the Scientific and Technological Research Equipment Center, Chulalongkorn University (STREC).

4.2.5 Infrared Spectroscopy (IR)

The functional groups in the samples were determined using Infrared spectroscopy. Before measurement, the sample was mixed with KBr and then was pressed to form a thin wafer. The equipment used was a Nicolet impact 400 at Center of Excellences on Catalysis and Catalytic Reaction Engineering, Chulalongkorn University.

4.3 Measurment of photocatalytic activity of catalysts

The apparatus and experimental procedures employed to evaluate the performance of various photocatalysts were described in this section.

4.3.1 Material

The reactant gas used for this study was ethylene in air as supplied by Thai Industrial Gas Limited. The gas mixture contained 0.1 vol % ethylene in balance air. Total flow rate of gas in the experiments was 15 ml/min.

4.3.2 Apparatus

Photoreactor system consists of a photoreactor and a gas controlling system.

4.3.2.1 Photoreactor

The photoreactor (see Figure 4.1) had two main components: an ultraviolet light source and the tubular packed bed reactor. The reactor was made from a Pyrex glass tube with a diameter of 5 mm and a length of 27 cm. The stainless steel tube is 1.5″ in length and 3/8″ in diameter connected to the both ends of the

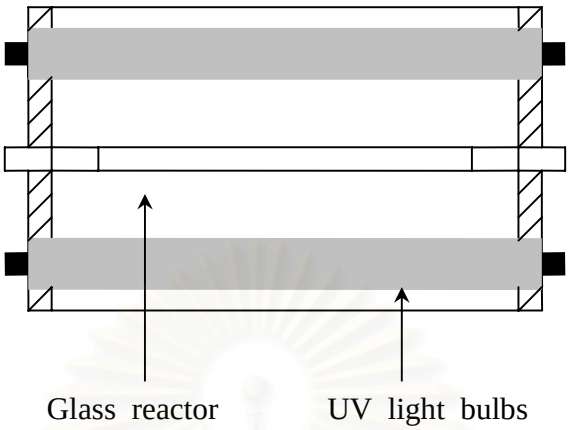

Figure 4.1 Photoreactor for experiments

reactor. Two sampling points were located on the left and right of catalyst bed. Photocatalyst was packed between two quartz wool layers.

Ultraviolet light sources were black light blue fluorescent bulbs (8 Watts). Four light bulbs were located 1.5 cm away from the reactor in square configuration. The photoreactor was covered with two layers of aluminum foil to minimize radiation losses from the system.

4.3.2.2 Gas Controlling System

Each feed line reactant was equipped with a pressure gauge and a ball valve. Flow rate of gas was adjusted using a metering valve and was measured using a bubble flow meter.

4.3.3 Experimental procedure for determining the activity of the photocatalyst

The photocatalytic activity was performed over 0.4 g of catalyst, which was packed in the reactor. The photoreactor was incorporated into the reactor system. Prior to

each experiment, the reactor was supplied with air at a flow rate of 15 ml/min. The photocatalyst was illuminated by ultraviolet light sources for one hour in order to remove any organic compounds that might remain from previous experiments from the surface of the catalyst. After one hour, the reactant, 0.1% (v/v) ethylene in air, was fed to the reactor at a flow rate of 15 ml/min. The temperature of the reactor under illumination was about 90°C, as measured using a K-type thermocouple. The flow rate of each gas was measured using a bubble flow meter. The diagram of the flow reactor system in order to test the photocatalysts was shown in Figure 4.2.

The effluent gas was sampled to measure the concentration of ethylene using GC-14B gas chromatrograph (Shimadzu), equipped with a flame ionization detector. The operating conditions for the instrument were listed in Table 4.1. The composition was measured every 20 minutes until steady state was achieved (as indicated by constant peak areas in the gas chromatograms).

Table 4.1 Operating conditions for gas chromatography

Gas Chromagraph	SHIMADZU GC-14B
Detector	FID
Column	VZ10
Carrier gas	H_2 (99.999%)
Carrier gas flow (ml/min)	30 cc/min
Column temperature	
- initial (^oC)	70
- final (^oC)	70
Injector temperature (^oC)	100
Detector temperature (^oC)	150
Current (mA)	-
Analysed gas	Hydrocarbon C_1-C_4

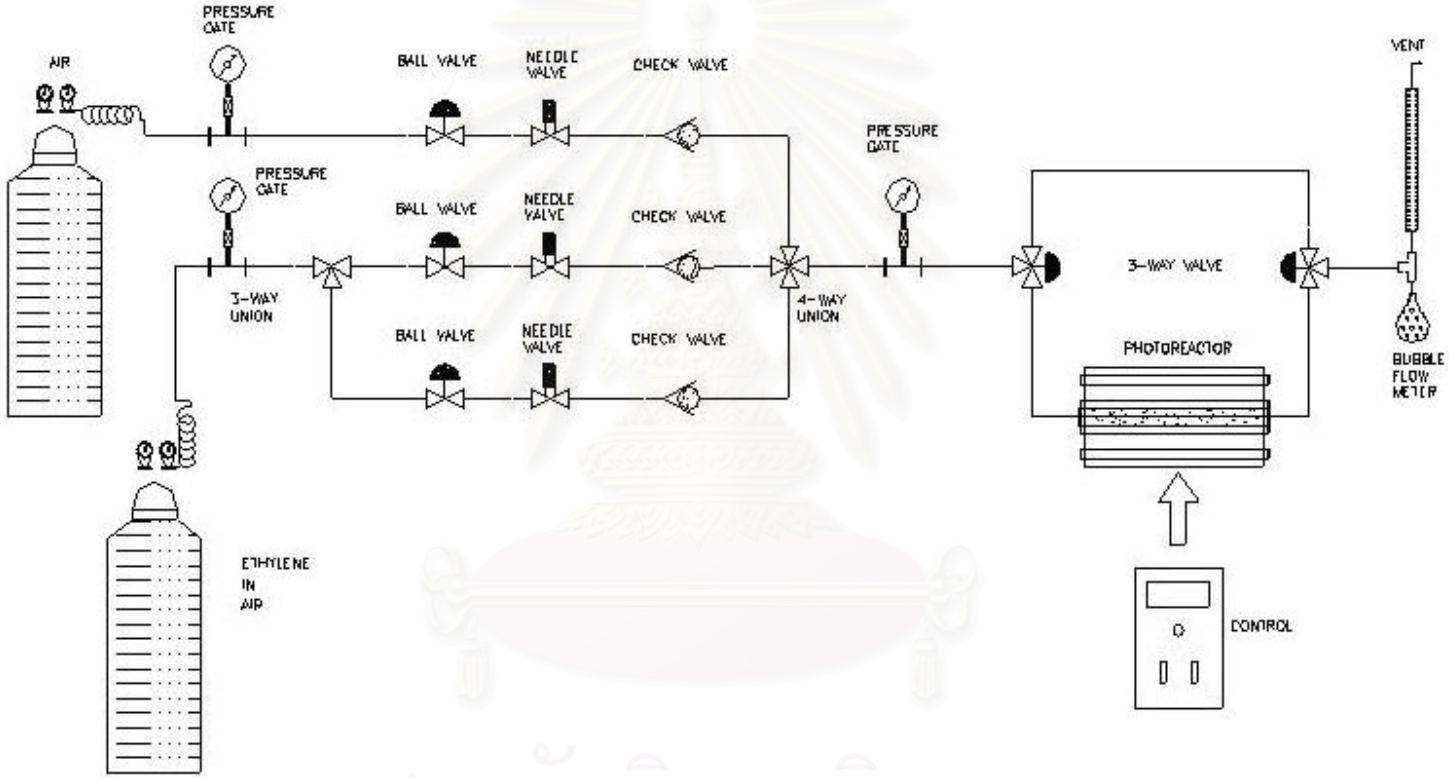

Figure 4.2 Flow diagram of photocatalytic oxidation of ethylene

CHAPTER V

RESULTS AND DISCUSSION

This chapter is divided into two parts. The first part presents experimental results from characterization and photocatalytic activity measurement of photocatalysts. The second part presents discussion on effects of calcination conditions and additions of second metal oxide to titanium dioxide.

5.1 Results

Experimental results involving titanium dioxide and four binary oxides, namely, titania-silica, titania-zirconia, titania-tin oxide, and titania-ceria, are presented.

5.1.1 Titanium dioxide as photocatalyst

5.1.1.1 Phase structures

The bulk crystalline phases of samples were determined using X-ray diffractometry (XRD). XRD patterns of TiO_2 after being calcined at four different temperatures, namely, 200°C, 320°C, 350°C, and 380°C, at holding times between 1 to 3 hours were displayed in Figures 5.1 to 5.3. Table 5.1 summarized crystal phase identification and approximate crystallite size of photocatalysts obtained from XRD. Average crystallite size (see Appendix A) was calculated from the line broadening of diffraction peak using the Scherrer formula. Rutile content (W_R) in terms of weight fraction was estimated from XRD intensity data of anatase and rutile peaks using Equation 5.1.

$$W_R = [1 + 0.8 I_A / I_R]^{-1} \qquad 5.1$$

Table 5.1 Summary of results obtained XRD analysis for titania under various calcination conditions.

Sample	Calcination		Crystal phase	Rutile content (%)	Crystallite size	
	temperature (°C)	time (hr)			anatase (nm)	rutile (nm)
A200-1	200	1	anatase	0	4.7	n/a
A200-2		2	anatase	0	5.1	n/a
A200-3		3	anatase	0	4.9	n/a
RA320-1	320	1	anatase + rutile	trace	5.0	-[a]
RA320-2		2	anatase + rutile	2.1	5.8	-[a]
RA320-3		3	anatase + rutile	3.8	6.4	-[a]
RA350-1	350	1	anatase + rutile	1.9	6.0	-[a]
RA350-2		2	anatase + rutile	4.1	6.4	-[a]
RA350-3		3	anatase + rutile	6.0	6.9	-[a]
RA380-1	380	1	anatase + rutile	5.4	6.5	-[a]
RA380-2		2	anatase + rutile	7.9	7.3	9.8
RA380-3		3	anatase + rutile	14.5	7.4	10.1

Note: -[a] Crystallite size of rutile could not be determined because the observed rutile peaks were too small.

I_A and I_R represented integrated intensities of anatase and rutile diffraction peaks, respectively. All calculated numbers for rutile content were included in Table 5.1.

As shown in Table 5.1, rutile content of the samples increased as calcination temperature increased. Similarly, when calcination time increased, rutile

content of titania became greater. Furthermore, anatase and rutile crystals grew continuously with increasing temperatures, as seen in the larger crystallite size at high

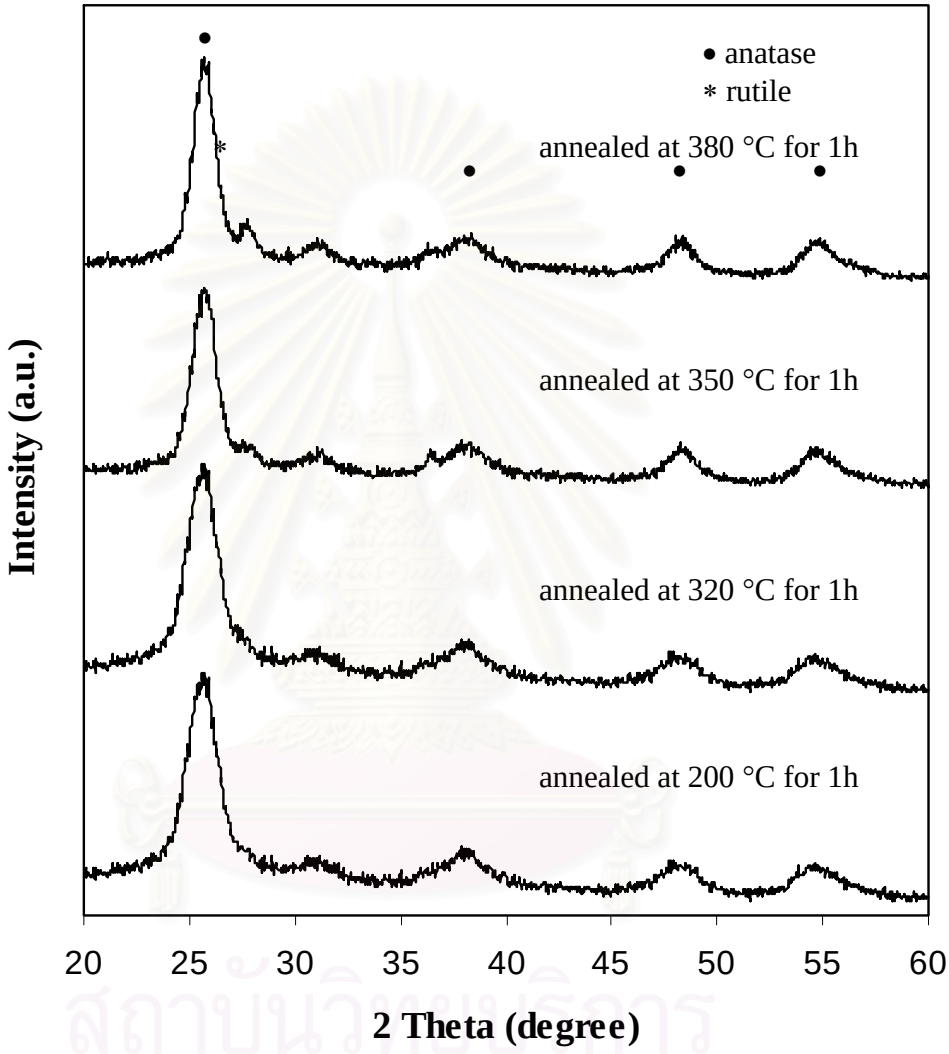

Figure 5.1 XRD patterns of titania calcined at different temperatures for a holding time of 1 hr.

calcination temperatures. The increase in crystallite size of titania was also observed when holding time in the furnace was increased.

From the crystalline structure of titania calcined at 200°C for one hour (see the Figure 5.1), the dominant peaks of anatase were at 2θ of about 25.2°, 37.9°, 47.8° and 53.8°, which represent the indices of (101), (004), (200) and (105) planes, respectively. No rutile phase was observed in titania calcined at this temperature. Nonetheless, partial phase transformation from anatase to rutile was

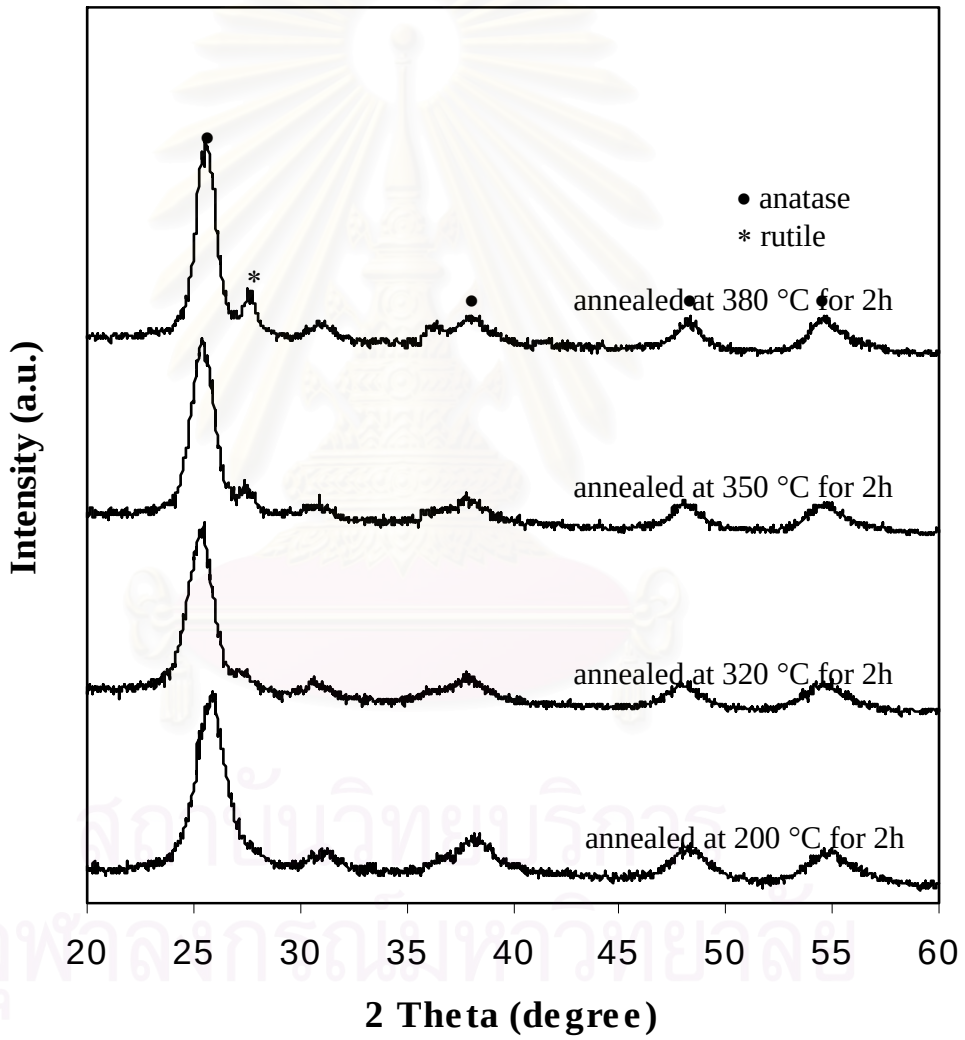

Figure 5.2 XRD patterns of titania calcined at different temperatures for a holding time of 2 hr.

observed in the samples calcined at temperatures above 320°C, resulting in the combination of anatase and rutile phases. The presence of rutile phase in the samples was identified by a dominant peak at 2θ of about 27.4°, which represented the index of (110) plane.

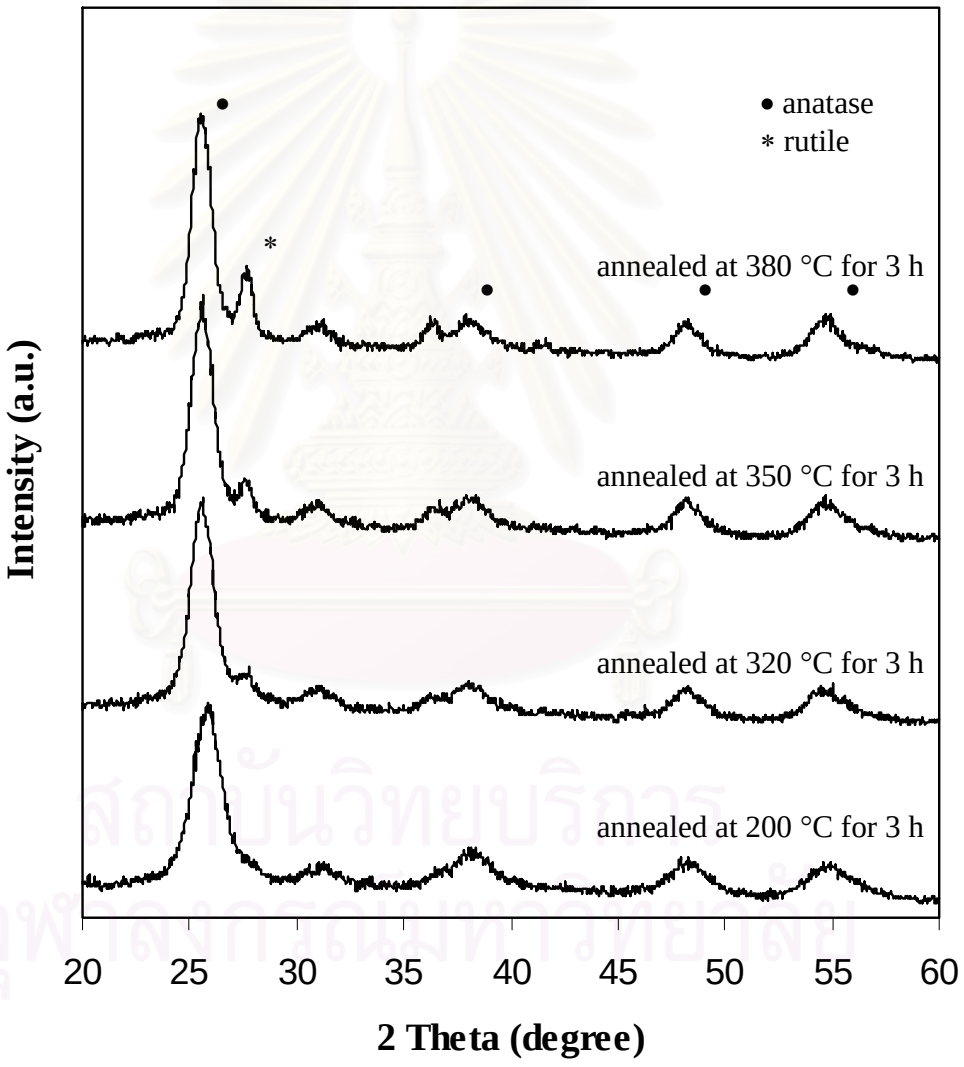

Figure 5.3 XRD patterns of titania calcined at different temperatures for a holding time of 3 hr.

Similarly, as shown in Figures 5.2 and 5.3, only anatase was found in the samples calcined at 200°C. When calcinations temperature was 320°C or higher, combination of anatase and rutile phase was detected in the samples.

5.1.1.2 BET surface areas and pore structure

In Table 5.2, the BET specific surface area, mean pore diameter, and total pore volume of titania were shown. These properties were determined from nitrogen adsorption isotherms. When either calcination temperature or time increased, specific surface area of titania decreased and so did total pore volume of the bulk material. In contrary, mean pore diameter became larger as either calcination temperature or time increased

Table 5.2 Summary of physical properties of the synthesized TiO_2, obtained from nitrogen adsorption measurement

Sample	Calcination		Specific surface area (m^2/g)	Mean pore diameter (nm)	Total pore volume (cm^3/g)
	temperature (°C)	time (hr)			
A200-1	200	1	245.5	4.9	0.300
A200-2		2	214.5	5.5	0.294
A200-3		3	195.1	4.6	0.224
RA320-1	320	1	160.0	4.0	0.228
RA320-2		2	142.7	6.4	0.227
RA320-3		3	136.6	6.7	0.161
RA350-1	350	1	155.4	6.6	0.256
RA350-2		2	136.6	6.4	0.217
RA350-3		3	126.7	7.5	0.238
RA380-1	380	1	130.7	6.3	0.208
RA380-2		2	115.2	7.1	0.205
RA380-3		3	101.6	7.9	0.200

5.1.1.3 Electron spin resonance (ESR)

The intensity of Ti^{3+} from ESR obtained from unheated TiO_2 powder at 77 K in vacuum as shown in Figure 5.4. The intensity of Ti^{3+} also decreased while the holding time increased at calcination temperature 200°C. On the other hand, the intensity of Ti^{3+} increased with increasing calcination temperature, namely, 320, 350 and 380°C and time for 1 to 3 h.

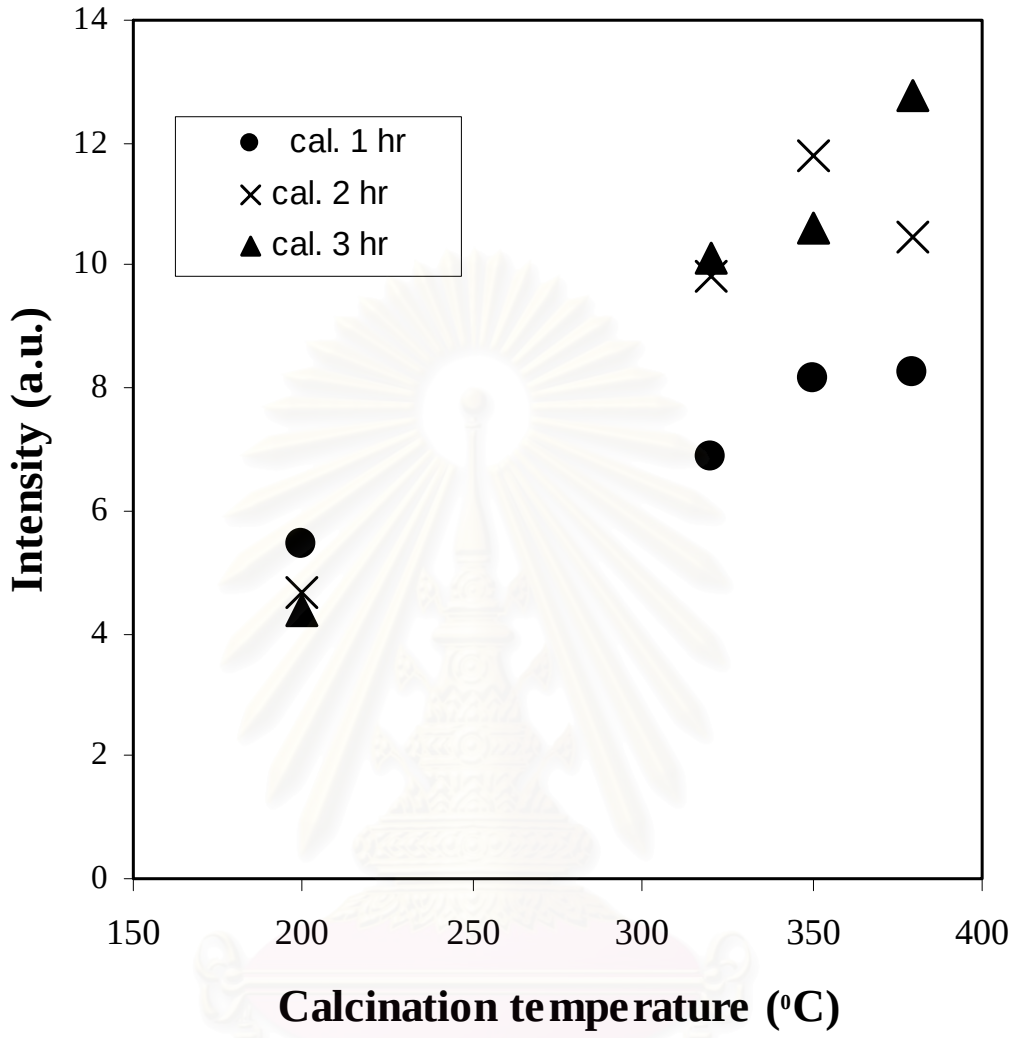

Figure 5.4 Intensity of Ti^{3+} peak in ESR spectrum for titanium dioxide under various calcinations conditions.

5.1.1.4 Photocatalytic oxidation reaction of ethylene

Titania nanoparticles were employed as catalysts in photocatalytic oxidation of ethylene. Time course for conversion of ethylene obtained from titania calcined at 200°C for one hour was displayed in Figure 5.5. Conversion of ethylene appeared to reach a steady state in less than one hour. Conversions of ethylene achieved from titania under various calcination conditions were displayed in Table 5.3. The photocatalytic activities of titanium dioxide decreased as either calcination time or

temperature increased. The highest photocatalytic activity achieved using titania fired at 200°C for one hour. When average crystallite size of anatase phase in the sample increased, either from higher calcination temperature or longer holding time, the achieved conversion of ethylene decreased (see Figure 5.6). Moreover, when specific surface area of sample increased, the conversion of ethylene also increased (see Figure 5.7). Inspection of Figure 5.8 suggested that the average conversion of ethylene also decreased when the rutile content became higher.

Table 5.3 Summary of photocatalytic activities of titania under various calcinations conditions for photocatalytic oxidation of ethylene in gas phase.

Sample	Calcination		Rutile content (%)	Crystallite size anatase (nm)	Specific surface area (m^2/g)	Average conversion of ethylene
	temperature (°C)	time (hr)				
A200-1	200	1	0	4.7	245.5	0.77
A200-2		2	0	5.1	214.5	0.71
A200-3		3	0	4.9	195.1	0.61
RA320-1	320	1	trace	5.0	160.0	0.60
RA320-2		2	2.1	5.8	142.7	0.60
RA320-3		3	3.8	6.4	136.6	0.54
RA350-1	350	1	1.9	6.0	155.4	0.60
RA350-2		2	4.1	6.4	136.6	0.52
RA350-3		3	6.0	6.9	126.7	0.47
RA380-1	380	1	5.4	6.5	130.7	0.53
RA380-2		2	7.9	7.3	115.2	0.48
RA380-3		3	14.5	7.4	101.6	0.41

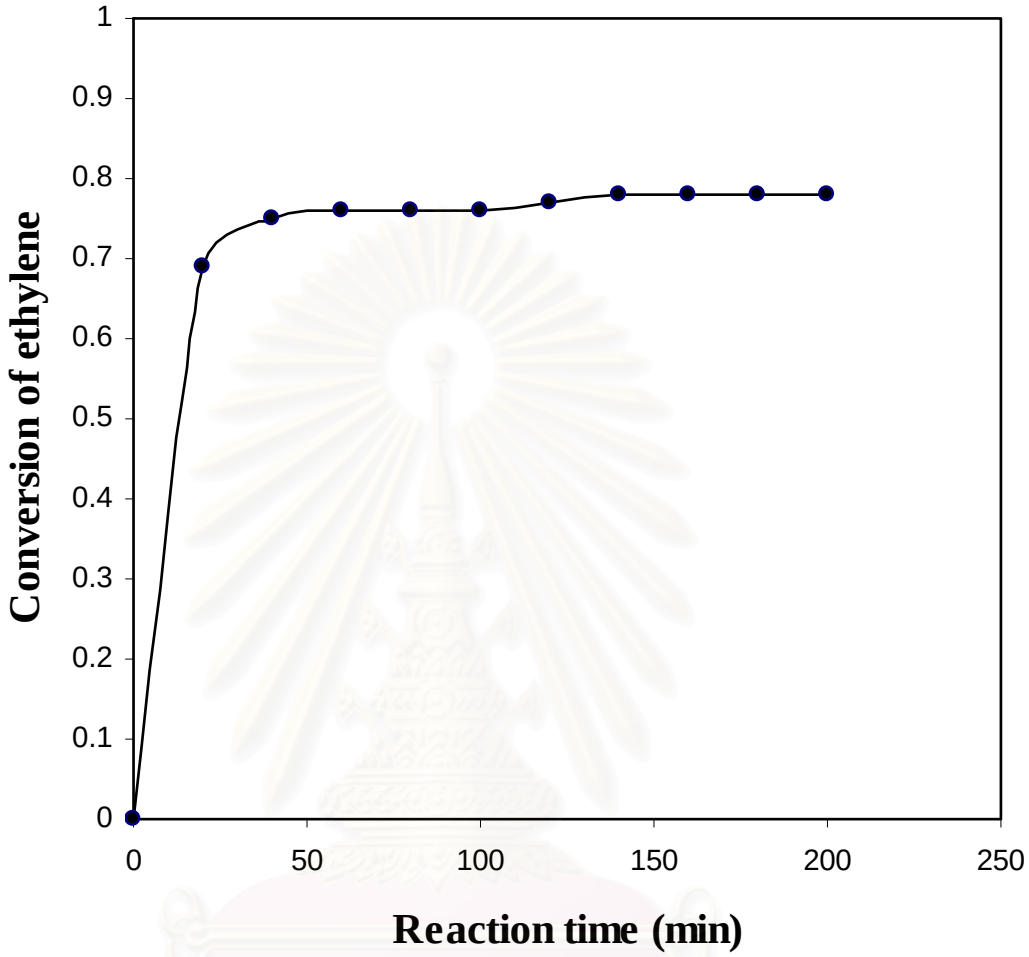

Figure 5.5 Time course for conversion of ethylene obtained from photocatalytic oxidation over titania calcined at 200°C for one hour.

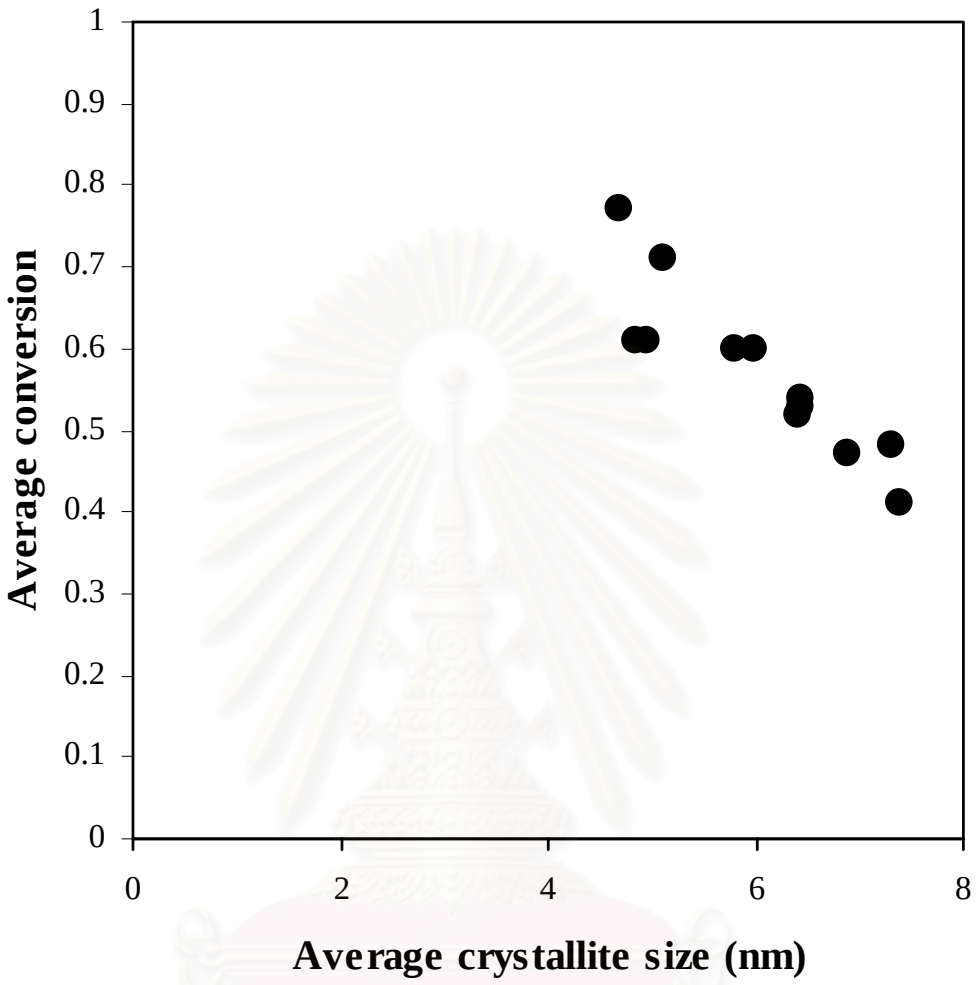

Figure 5.6 Average conversion of ethylene achieved in photocatalytic oxidation over titanium dioxide nanoparticles as a function of average crystallite size of anatase in the sample.

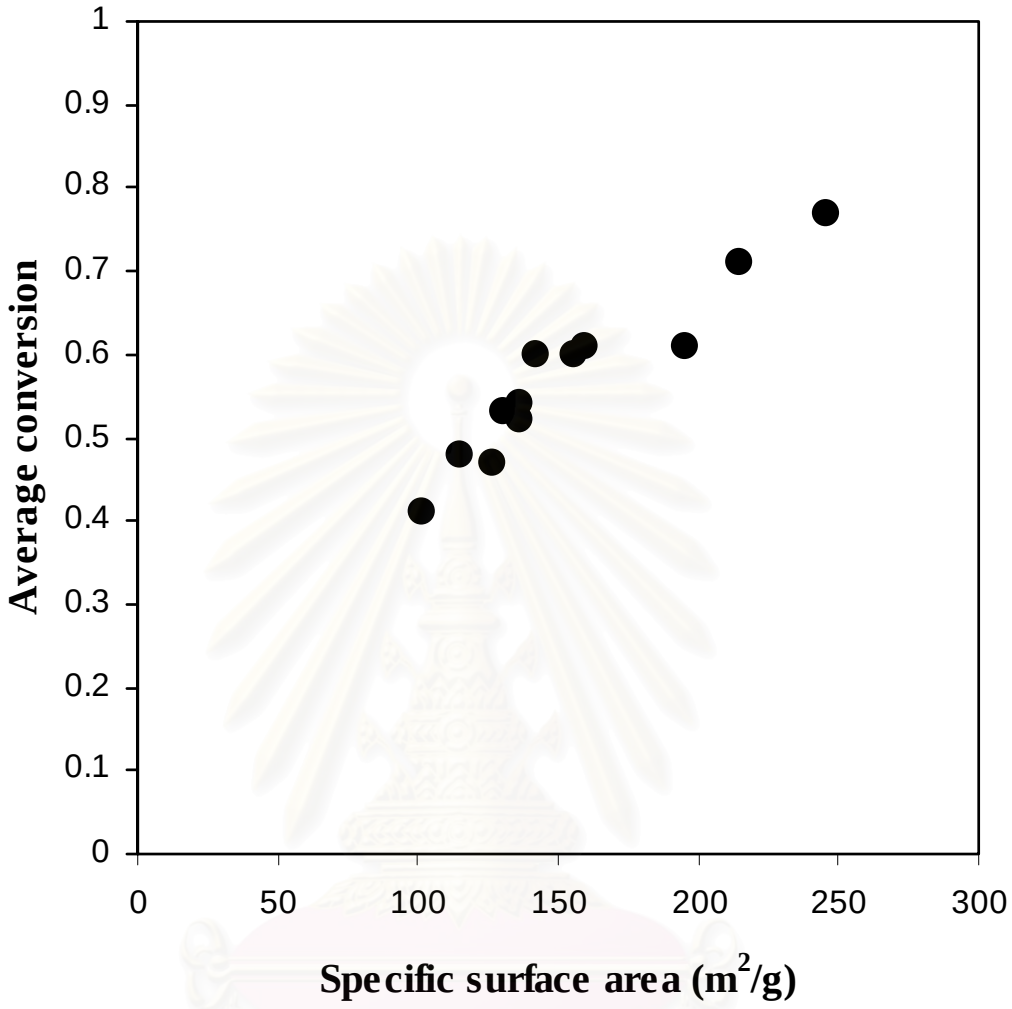

Figure 5.7 Average conversion of ethylene achieved in photocatalytic oxidation over titanium dioxide nanoparticles as a function of surface area of anatase in the sample.

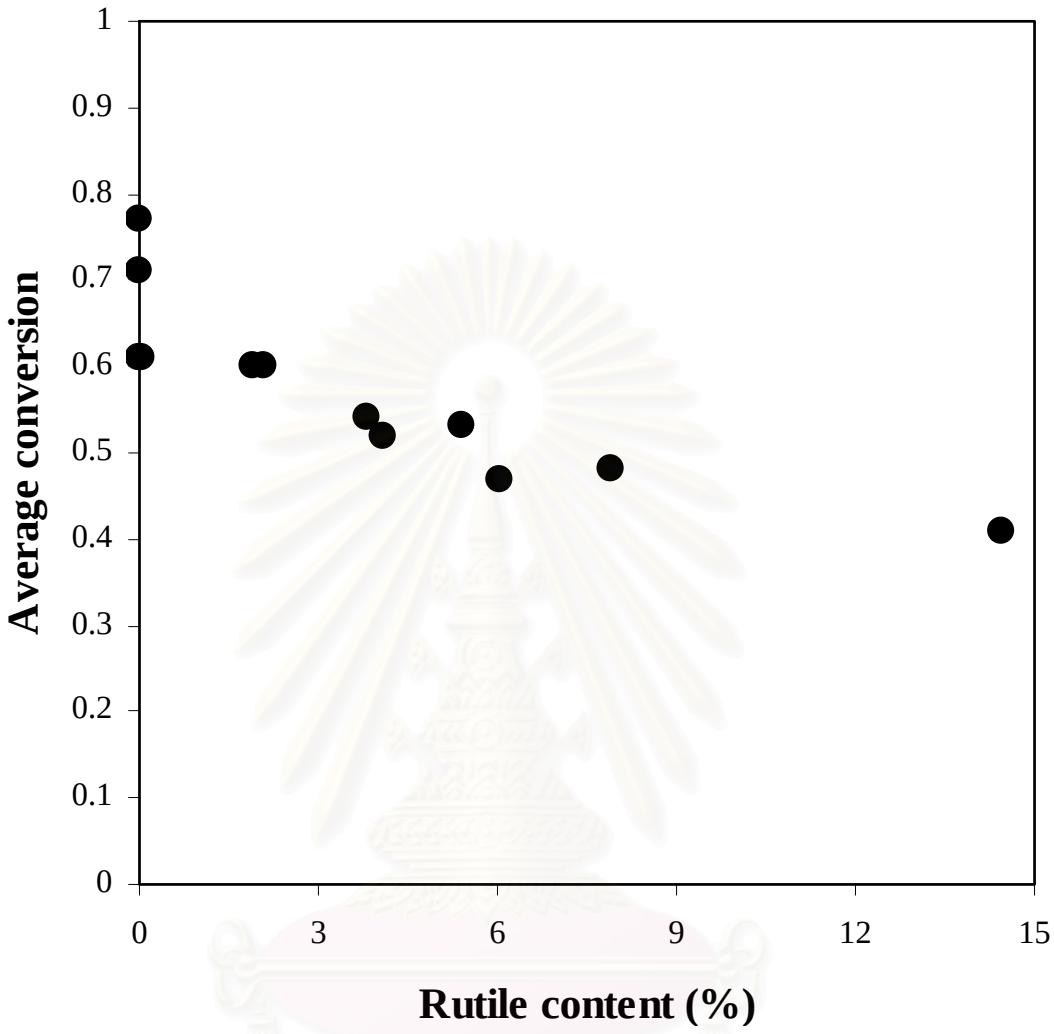

Figure 5.8 Average conversion of ethylene achieved in photocatalytic oxidation over titanium dioxide nanoparticles as a function of fraction of rutile phase present in the sample.

5.1.2 Binary mixed oxide

Four types of binary mixed oxide, *i.e.*, SiO_2-TiO_2, ZrO_2-TiO_2 , SnO_2-TiO_2, CeO_2-TiO_2, were prepared and were employed as photocatalysts (see Section 4.1.2).

Results from various characterization techniques and measurements of photocatalytic activities for those metal oxides were presented.

5.1.2.1 Composition and crystal phase structure

XRF was performed to determine the composition of each metal oxide in the bulk of catalysts. The content of second metal oxide in TiO_2-rich binary oxides were show in table 5.4.

Table 5.4 Summary of results obtained for XRF and XRD analysis for binary metal oxides at calcination temperature of 200°C for one hour.

Sample	Calcination		Second metal oxide content (wt %)	Crystal phase of TiO_2	Crystallite size anatase (nm)
	temperature (°C)	time (hr)			
TiO_2	200	1	0	anatase	4.5
SiO_2-TiO_2	200	1	9.3	anatase	3.6
ZrO_2-TiO_2	200	1	10.7	anatase	4.3
SnO_2-TiO_2	200	1	5.3	anatase	3.8
CeO_2-TiO_2	200	1	0.8	anatase	4.3

The XRD patterns of pure TiO_2 and four binary metal oxides were displayed in Figure 5.9. Only diffraction peaks that corresponded to anatase titania were observed. No peaks corresponding to silica, zirconia**,** tin dioxide or ceria crystals appeared in the XRD patterns. Therefore, second metal oxide existed in amorphous form for all binary oxides. Moreover, peaks of anatase in the CeO_2-TiO_2 mixed oxide appeared sharper than those in pure titania owing to higher crystallinity of anatase phase in the sample.

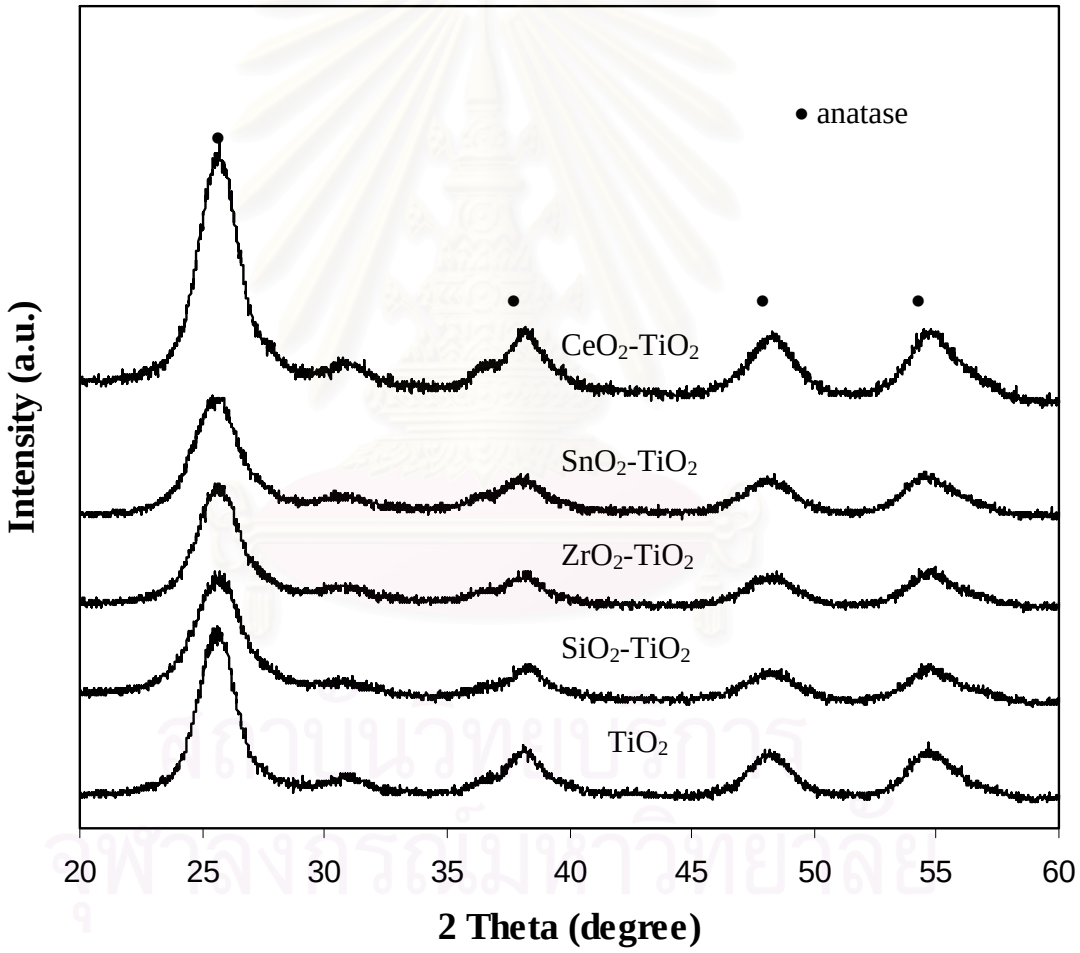

Figure 5.9 XRD patterns of pure TiO_2 and four binary oxides that were calcined at 200°C for one hour.

The crystallite sizes of mixed oxides were smaller than that of pure titania (see Table 5.4) of various binary mixed oxides. The crystallite size of SiO_2-TiO_2 mixed oxide was the smallest one.

5.1.2.2 Specific surface areas

Specific surface areas of titania and four binary metal oxides that were calcined at 200°C for one hour were shown in Table 5.5. Since specific surface areas of binary metal oxides were larger than that of pure titania. Addition of second metal oxide to titania could increase specific surface area of the resulting oxide.

Table 5.5 Specific surface area of titania and four binary oxides that were calcined at 200°C for one hour.

Sample	Calcination		Metal oxide (wt%)	Specific surface area (m^2/g)
	temperature (°C)	time (hr)		
TiO_2	200	1	0	147.3
SiO_2-TiO_2	200	1	9.3	182.2
ZrO_2-TiO_2	200	1	10.7	183.0
SnO_2-TiO_2	200	1	5.3	170.7
CeO_2-TiO_2	200	1	0.8	172.2

5.1.2.3 Electron spin resonance spectroscopy (ESR)

Table 5.6 Intensities of Ti^{3+} peak from ESR spectra for titania and four binary metal oxides that were calcined at 200°C for one hour.

Sample	Metal oxide (wt %)	Intensity of Ti^{3+}
TiO_2	0	5.4
SiO_2-TiO_2	9.3	7.0
ZrO_2-TiO_2	10.7	11.3
SnO_2-TiO_2	5.3	23.2
CeO_2-TiO_2	0.8	3.6

5.1.2.4 Fourier transform Infrared Spectroscopy (FT-IR)

Figure 5.10 showed the FT-IR spectra for different types of metal oxides, namely, SiO_2-TiO_2, ZrO_2-TiO_2, SnO_2-TiO_2 ,CeO_2-TiO_2, and pure TiO_2, that were calcined at 200 °C for one hour. A peak at the wavenumber near 3400 cm^{-1}, which corresponded to a stretching vibration of Ti-OH group, was observed in every sample. At a wavenumber of 1620 cm^{-1}, a band assigned to water also appeared.

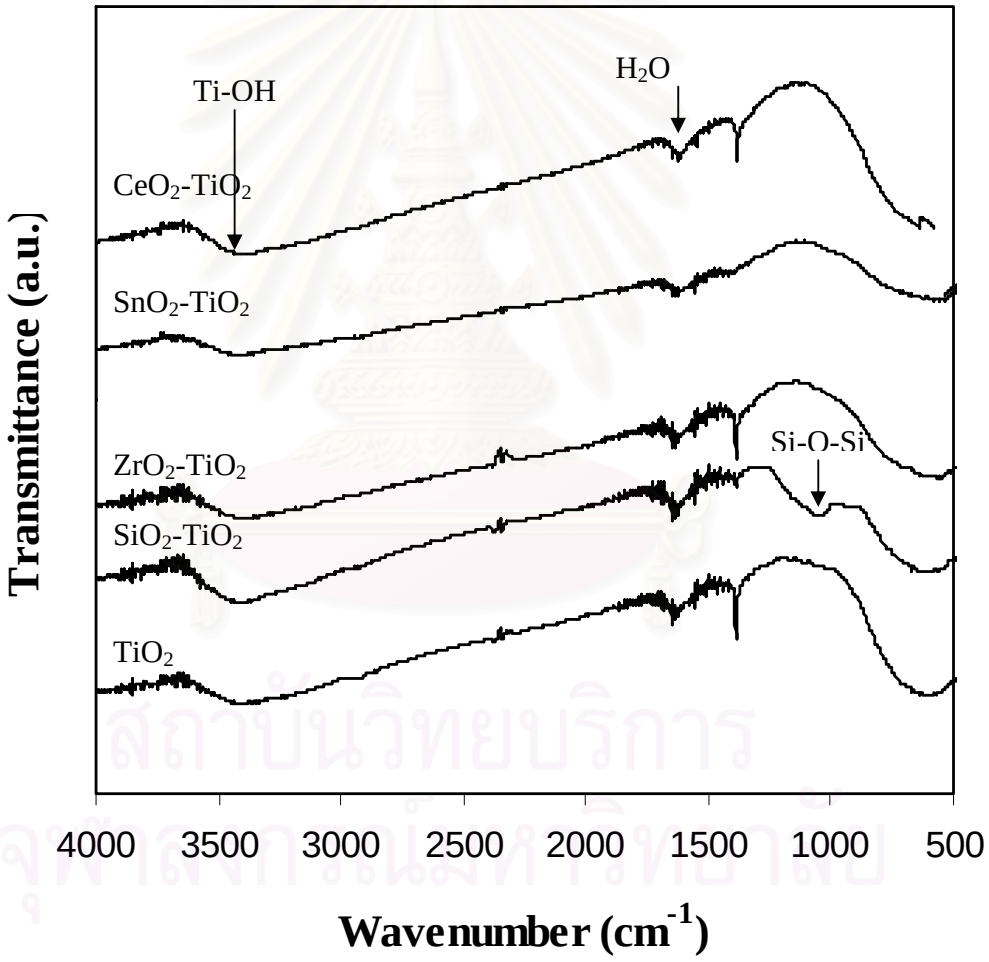

Figure 5.10 FT-IR spectra of the pure TiO_2 and four binary metal oxides that were calcined at 200°C for one hour.

In SiO_2-TiO_2 mixed oxide, a band for Si-O-Si bond at wave number between of 1080 and 1105 cm^{-1} was detected, whereas the Si-O-Ti bond at the wavenumber of 940-960 cm^{-1} were not observed.

5.1.2.5 Photocatalytic activities for oxidation reaction of ethylene over various metal oxides.

The photoactivities of pure TiO_2 and four binary oxides namely, SiO_2-TiO_2, ZrO_2-TiO_2, SnO_2-TiO_2 and CeO_2-TiO_2, that were calcined at 200 °C for one hour were determined for photocatalytic oxidation of ethylene and were displayed in Table 5.7. The results indicated that pure TiO_2 possessed the highest photoactivity. All of the binary mixed oxides had lower photoactivity than that of pure TiO_2 despite having larger specific surface areas

Table 5.7 Summary of photocatalytic activity of titania and four binary oxides that were fired at 200°C for one hour.

Sample	Metal Oxide (wt %)	Crystallite size anatase (nm)	Specific surface area (m^2/g)	Average conversion of ethylene	Intensity of Ti^{3+}
TiO_2	0	4.5	147.3	0.77	5.4
SiO_2-TiO_2	9.3	3.6	182.2	0.52	7.0
ZrO_2-TiO_2	10.7	4.3	183.0	0.64	11.3
SnO_2-TiO_2	5.3	3.8	170.7	0.62	23.2
CeO_2-TiO_2	0.8	4.3	172.2	0.14	3.6

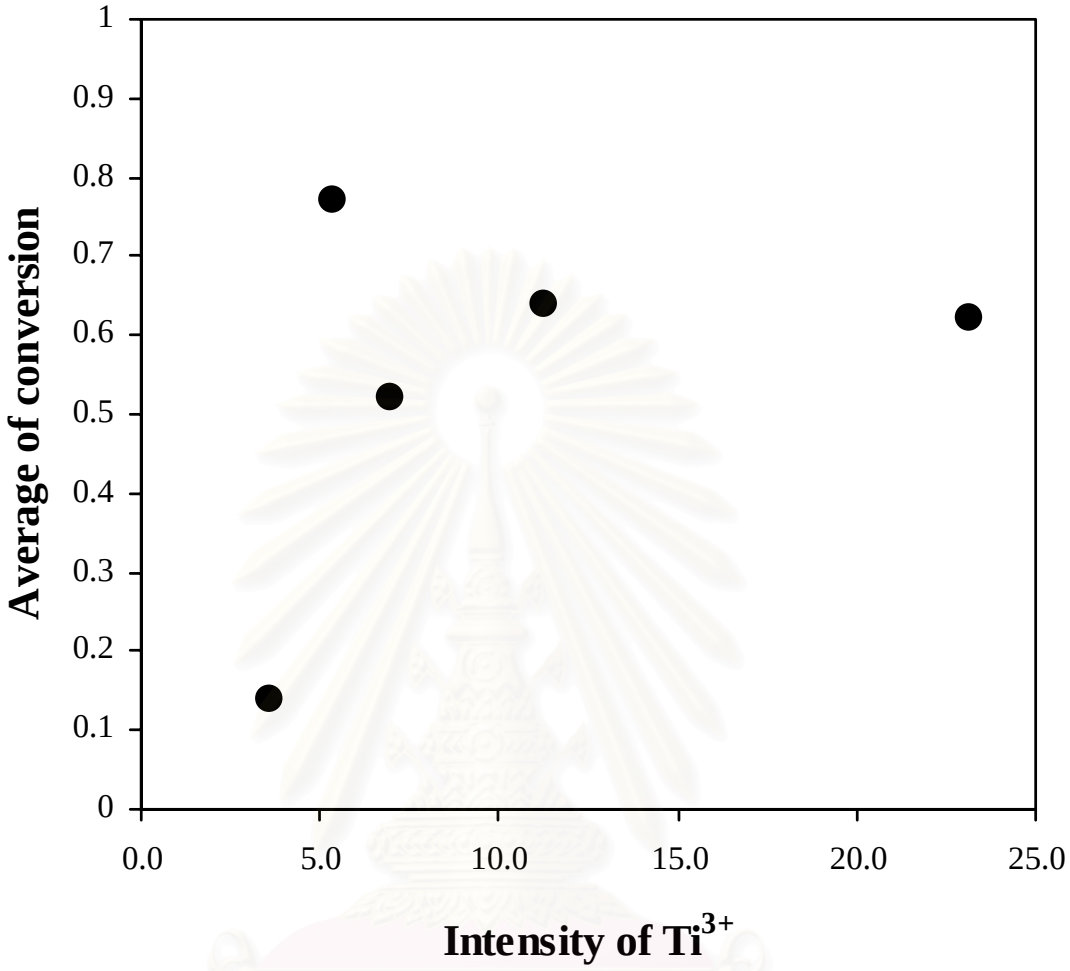

Figure 5.11 The average conversion of ethylene as a function of the intensity of Ti^{3+}

When we plotted the average conversion of ethylene as a function of the intensity of Ti^{3+} peak in ESR spectrum (see Figure 5.11), one did not observe any correlation between the two parameters.

5.2 Discussion

In this section, experimental results from the previous section were discussed. First, results involving pure titania were discussed in Section 5.2.1 And discussion about results involving binary metal oxides was presented in Section 5.2.2.

5.2.1 Titanium dioxide

Photocatalytic oxidation of ethylene in gas phase were employed to investigate photocatalytic activity of titania prepared by a sol-gel under various calcination conditions. Titania that was calcined at 200°C for one hour exhibited the highest conversion in the photocatalytic oxidation of ethylene as seen in Table 5.3. At a calcination temperature of 200°C, titania crystal existed as anatase phase without contamination from rutile phase. When calcination time increased, the conversion of ethylene decreased while crystallite size of anatase increased. The reason for the higher conversions obtained from catalyst with small crystallite sizes was mainly the increase in specific surface area of the catalyst. Similar behaviors have been reported for gas phase photocatalytic oxidation of toluene (Maira *et al.*, 2001), ethylene (Park *et al.*, 1999), and trichloroethylene (Maira *et al.*, 2000; Nishida *et al.*, 1993; Anderson *et al.*, 1993) over titania photocatalysts. Furthermore, increasing either calcination time or temperature gave rise to loss in specific surface area, which was attributable to pore coalescence from crystallization of walls that separated mesopores. Consequently, this phenomenon caused an increase in mean pore diameter and a decrease in total pore volume of the bulk materials (Seethawong *et al.*, 2005). A reduction in specific surface area resulted in fewer numbers of active surface sites, which were available for reactants such as ethylene to adsorb onto and react with photogenerated charge carriers. Inspection of Figure 5.4 indicated that the intensity of Ti^{3+} peak in ESR spectrum for titania fired at 200°C for one hour was the highest. Greater amounts of Ti^{3+} gave rise to higher photocatalytic activity of titania (Maira *et al.*, 2001). When calcination time increased, smaller specific surface area and smaller amounts of Ti^{3+} in titania occurred as a result. As the size of particles for titania decreased, the proportion of edge and corner sites to the planar sites increased (Maira *et al.*, 2001). The species (*i.e.*, Ti^{4+} or O_2^-) at the edge and corner had lower coordination numbers and were expected to exhibit different catalytic and adsorption properties when compared to the planar atoms. The smaller titania particles, which were calcined 200°C for one hour, had fewer planar sites that trapped photogenerated holes at a subsurface location, whereas the greater amount of edge and corner sites in titania

allowed the formation of Ti^{3+} centers where oxygen molecules could chemisorb and could form superoxide ions (i.e. $Ti^{3+}_{(surface)} + O_2 \rightarrow Ti^{4+} + O_2^-$). These chemical species formed by the interactions of electron and holes with the lattice atoms and chemisorbed oxygen may be responsible for excellent performance of titania that was calcined at 200°C for one hour as photocatalyst for degradation of ethylene. Similar results were reported in the degradation of photooxidation of toluene in gas phase (Maira *et al.*, 2001). Calcination of titania at 320°C, 350°C, and 380°C resulted in a combination of anatase and rutile phases in the catalysts (see Table 5.1). For these titania particles, the amount of Ti^{3+} became greater as calcination temperature or time increased (see Figure 5.4)

In spite of greater amount of Ti^{3+} in titania, higher conversions of ethylene were observed in titania calcined at lower temperature or for shorter duration. This observation suggested other parameters played more significant roles in the photocatalytic activity for degradation of ethylene than the amount of Ti^{3+}. Figure 5.8 showed the dependence of photodegradation of ethylene on rutile content of titania. The conversion of ethylene decreased as the rutile ratio increased. The presence of rutile phase in titania caused detrimental effect on photocatalytic activity (Hoffman *et al.*, 1995; Karakitsou *et al.*, 1993; Ichikawa *et al.*, 1997). This negative effect may be attributed to a lower flat band potential of rutile. Furthermore, specific surface seemed to have significant effect on the photocatalytic activities for the reason mentioned above. Inspection of Figure 5.7 indicated the average conversion of ethylene was inversely proportional to the specific surface area of titania.

5.2.2 Binary mixed oxide

Conversions of ethylene over pure TiO_2 and four binary metal oxides that were fired at 200°C for one hour were reported in Table 5.7. The conversion of ethylene over pure TiO_2 was the highest value at 77 %. Adding the second metal oxides, namely, SiO_2, ZrO_2, SnO_2, and CeO_2 to TiO_2 led to lower photocatalytic activities.

For SiO_2-TiO_2 mixed oxide, addition of silica to titania inhibited the transformation of titania from amorphous to anatase (Xie *et al.*, 2004). Excessive amount of silica added could lead to active surface sites of titania being covered by inactive silica. Furthermore, inspection of FTIR spectrum of SiO_2-TiO_2 mixed oxide revealed a band for Si-O-Si vibration (see Figure 5.10). This finding suggested that silica existed as a segregated amorphous phase and was not incorporated into anatase titania. Since the presence of Ti-O-Si bond was believed to enhance photocatalytic activity of mixed oxide, the lack of such bond could lead to low photocatalytic activity (Xie *et al.*, 2004).

Our results for SiO_2-TiO_2 mixed oxide did not agree with several researchers who reported higher photocatalytic activity of SiO_2-TiO_2 mixed oxide than that of pure TiO_2 (Zhang *et al*., 2001; Liu *et al*., 2004; Jung and Park, 1999; Cheng *et al.*, 2003; Xie *et al*., 2004). The enhancement in photocatalytic activity was attributed to larger specific surface area and strong surface acidity (Zhang *et al*., 2001) or an increase in oxygen vacancies (Cheng *et al*., 2003). However, Jung and Park (2004) reported lower activity for ZrO_2-TiO_2 despite larger specific surface than that of TiO_2. They attributed the observation to reduction in pore size, which could lead to difficulty for reactants to diffuse to the active surface. Our speculation was that the lower activity observed was a result of the same phenomenon.

For SnO_2-TiO_2 mixed oxide, the lower photocatalytic activity for mixed oxide was in agreement with work done by Shang and coworkers (2004). This result was attributed to greater recombination rate of photogenerated electrons and holes in SnO_2-TiO_2 mixed oxide.

The lower photocatalytic activity for CeO_2-TiO_2 mixed oxide was attributed to larger isoelectric point of the mixed oxide (Lin and Yu, 1998). High isoelectric point led to fewer hydroxide ions on the surface of catalyst. Hydroxide ion acted as traps for holes to prevent recombination of electrons and holes.

As mentioned in previous section, Ti^{3+} appeared to have significant effect on photocatalytic activity of titania. Nonetheless, there seemed to be no correlation between photocatalytic activity of mixed oxides and amount of Ti^{3+}. Other parameters discussed above might play more significant role in determining photocatalytic activity of binary metal oxides.

CHAPTER VI

CONCLUSIONS AND RECOMMENDATIONS FOR FUTURE RESEARCH

This chapter summarizes experimental results involving characterization of titania and binary metal oxides for studies of the photocatalytic oxidation of ethylene. Recommendations for future research are also presented.

6.1 Conclusions

This research was divided into two parts. The first part involved the characterization and utilization of titania as photocatalyst. The second part involved binary metal oxides.

6.1.1 Titanium dioxide as photocatalyst

Titania nanoparticles were prepared via a sol-gel method under various calcination conditions (*i.e.*, temperature and time). Photocatalytic oxidation of ethylene was employed as a probe reaction. Only anatase phase was observed for titania samples that were calcined at 200 °C although both anatase and rutile phases were found in the samples that were calcined at 320 °C or higher. When calcination temperature or time increased, crystallite size of titania became larger and rutile content increased. The highest conversion of ethylene was obtained using titania that was calcined at 200 °C for one hour. This finding can be attributed to large specific surface area of titania and the absence of rutile phase. Moreover, the results also suggested that the amount of Ti^{3+} in the catalyst could be indicative of photocatalytic activity of titania with only anatase phase present.

When both anatase and rutile were present in titania, there seemed to be no correlation between the amount of Ti^{3+} and activity of titania photocatalyst. Other factors

such as specific surface area and rutile content might have more significant effects on the activity.

6.1.2 Binary metal oxide as photocatalyst

Four different binary oxides, namely, SiO_2-TiO_2**,** ZrO_2-TiO_2**,** SnO_2-TiO_2, and CeO_2-TiO_2**,** were prepared using a sol-gel method. Photocatalytic activities of the binary oxides were measured using pohotooxidation of ethylene as a probe reaction. Adding the second metal oxide to titania lowered the activity of mixed oxides as photocatalysts. Although no rutile phase was found in the mixed oxides, there seemed to be no correlation between the amount of Ti^{3+} in the sample and photocatalytic activity. Other factors such as crystal phases and structures should be considered when attempting to determine photocatalytic activity of mixed oxide.

6.2 Recommendations for future research

1. Effect of amount of second metal oxide in the binary metal oxide should be further investigated in order to determine the optimal composition of the mixed oxide, which gives rise to in high activities for photocatalytic oxidation.

2. Improvement of the method of preparation for the binary metal oxide should be further studied.

REFERENCES

Abdullan, M., Low, G.K.-C., and Matthews, R.W. Effects of common inorganic anions on rates of photocatalytic oxidation of organic carbon over illuminated titanium dioxide. J. Phys. Chem. 94 (1990): 6820-6825.

Alherici, R.M., and Jardim, W.F. Photocatalytic destruction of VOCs in the gas phase using titanium dioxide. Appl. Catal. B 14 (1997): 55-68.

Anderson, M., Nishida, S., March, S., and Ekabi. H. Photocatalytic purification and treatment of water and air, Elsevier, Amsterdam . (1993): 405.

Bamwenda, R., and Arakawa, H. Cerium dioxide as a photocatalyst for water decomposition to O_2 in the presence of Ce^{4+}_{aq} and Fe^{3+}_{aq} species. J.of Mole. Catal.A:Chem. 161 (2000):105-113.

Bamwenda, R., Useigi, T., Abe, Y., Sayama, K., and Arakawa, H. The photocatalyticoxidation of water to O_2 over pure CeO_2, WO_3, and TiO_2 using Fe^{3+} and Ce^{4+} as electron acceptors. J.Appl.Catal.A:Gene. 205 (2001): 117-128.

Belhekar, A., Awate, V., and Anand, R. Photocatalytic activity of titania modified mesoporous silica for pollution control. Catal.Commu. 3 (2002): 453-458.

Botta, S.G., Navio, J.A., Hidalgo, M.C., Restrepo, G.M., and Litter, M.I. Photocatalytic properties of ZrO2 and Fe/ZrO2 semiconductors prepared by a sol-gel technique. J. Photochem. Photobiol. A: Chem. 129 (1999): 89-99.

Calza, P., Minero, C. and Pelizzetti, E. Photocatalytically assisted hydrolysis of chlorinated methanes under anaerobic conditions. Environ. Sci. Techol. 31 (1997): 2198-2203.

Cheng, P., Zheng, M., Jin, Y., Juang, Q., and Gu, M. Preparation and characterization of silica-doped titania photocatalyst though sol-gel method. Mater.Lett. 57 (2003): 2989-2999.

Coronado, M., Maira, A., Arias, A., Conesa, J., and Soria, J. EPR study of the radicals formed upon UV irradiation of ceria-based photocatalysts. J. Photochem. and Photobiol. A: Chem. 150 (2002): 213-222.

Deng, X., Yue, Y., and Gao, Z. Gas-phase photo-oxidation of organic compounds over nanosized TiO_2 photocatalysts by various preparations. Appl. Catal. B: Enviro.39 (2002): 135-147.

Fox, M. A., and Dulay, M. T. Heterogeneous photocatalysis. Chem. Rev. 93 (1993): 341-357.

Francisco, M., and Mastelaro, V. Inhibition of the anatase-rutile phase transformation with addition of CeO2 to CuO-TiO2 system:Raman spectroscopy, X-ray diffraction, and textural studies. Chem. Mater. 14 (2002):2514-2518.

Fujishima, A., Hashimoto, K., and Watanabe, T., TiO_2 photocatalysis: fundamental and applications. 1st ed. Tokyo: BKC, 1999.

Fu, X., Clark, L., Zeltner, W., and Anderson , A. Effects of reaction temperature and water vapor content on the heterogeneous photocatalytic oxidation of ethylene. J. Photochem. Photobiol. A: Chem. 97 (1996): 181-186.

Gao, L., and Zhang, Q. Effects of amorphous contents and particle size on the photocatalytic properties of TiO_2 nanoparticles. Scripta mater. 44 (2001): 1195-1198.

Hirano, M., Nakahara, C., Ota, K., Tanaike, O., and Inagaki, M. Photoactivity and phase stability of ZrO_2-doped anatase-type TiO_2 directly formed as nanometer-sized particles by hydrolysis under hydrothermal conditions.
J. Solid. State. Chem.170 (2003): 39-47.

Hoffmann, M., Martin, S., choi, W., and Bahnemann, D. Enviromental applications of semiconductor photocatalysis. Chem. Rev. 95 (1995): 69-96.

Hong, S., Lee, M., Park, S., and Lee, G. Synthesis of nanosized TiO_2/SiO_2 particles in the microemulsion and their photocatalytic activity on the decompsiton of *p*-nitrophenol. Catal. Today. 87 (2003): 99-105.

Ichikawa, S., and Doi, R. Photoelectrocatalytic hydrogen production from water on transparent thin film titania of different crystal structures and quantum efficiency characteristics. Thin Solid Films. 292 (1997): 130-134.

Jung, K., and Park. S. Anatase-phase titania:preparation by embedding silica and photocatalytic activity for the decomposition of tirchloroethylene. J.Photochem and Photobiol.A:Chem. 127 (1999): 117-122.

Jung, K., and Park, S. Photoactivity of SiO_2/TiO_2 and ZrO_2/TiO_2 mixed oxides prepared by so-gel method. Mater. Lett. 58 (2004): 2897-2900.

Jung, K., and Park, S., and Anpo, M. Photoluminescence and photoactivity of titania particles prepared by the sol-gel technique: effect of calcination temperature. J. Photochem. Photobiol.A: Chem. 170 (2004) 247-252.

Karakitsou, K., and Verykios, X. Effects of altervalent cation doping of titania on its performance as a photocatalyst for water cleavage. J. Phys. Chem. 97 (1993): 1184-1189.

Kominami, H., Murakami, S.-Y., Kohono, M., Kera, Y., Okada, K. and Ohtani, Stoichiometric decomposition of water by titanium (IV) oxide photocatalyst synthesized in organic media: Effect of synthesis and irradiation conditions on photocatalytic activity. J. Phys. Chem. 3 (2001): 4102-4106.

Li, Y., White, T., and Lim, S. Structure control and its influence on photoactivity and phase transformation of TiO_2 nano-particles. Rev. Adv. Mater. Sci. 5 (2003): 211-215.

Lin, J., and Yu, J. An investigation on photocatalytic activities of mixed TiO_2-rare earth oxides for the oxidation of acetone in air. J. Photochem. Photobiol. A: Chem. 116 (1998): 63-67.

Lin, J., Yu, J., Lo, D., and Lam, S. Photocatalytic activity of rutile $Ti_{1-x}Sn_xO_2$. J. Catal. 183 (1999):368-379.

Linsebigler, A. L., Lu, G. and Yates, Jr. J. T. Photocatalysis on TiO_2 surfaces: principles, mechanism, and selected results. Chem. Rev. 95 (1995): 735-758.

Litter, M.L. Heterogeneous photocatalysis transition metal ions in photocatalytic systems. Appl. Catal. B: Environ. 23 (1999): 89-114.

Liu, Z., Quan, X., Fu, H., Li, X., and Yang, K. Effect of embedded-silica on microstructure and photocatalytic activity of titania prepared by ultrasound-assisted hydrolysis. Appl. Catal. B: Environ. 52 (2004): 33-40.

Maira, A., Yeung, K., Lee. C., Yue, P., and Chan, C. Size effects in gas-phase photo-oxidation of trichloroethylene using nanometer-size TiO_2 catalysts. J. Catal. 192 (2000): 185-196.

Maira, A., Yeung, K., Soria, J., Coronado, J., Belver, C., Lee, C., and Augugliaro, V. Gas-phase photo-oxidation of toluene using nanometer-size TiO_2 catalysts. Appl.Catal.B:Enviro. 29 (2001): 327-336.

Mills, A. and Wang, J. Photomineralisation of 4-chlorophenol sensitized by TiO_2 thin films. J. Photochem. Photobiol. A: Chem. 118 (1998): 53-

Nakaoka, M., and Nosaka, Y. ESR investigation into the effects of heat treatment and crystal structure on radicals produced over irradiated TiO_2 powder. J. Photochem. Photobiol. A: Chem. 110 (1997): 299-305.

Nam, W., and Han, G. Characterization and photocatalytic performance of nanosize TiO_2 powders prepared by the solvothermal method. Korea J. chem. Eng. 20 (2003): 1149-1153.

Navio, J.A., Colon, G., and Herrmann, J.M. Photoconductive and photocatalytic properties of $ZrTiO_4$. Comparison with the parent oxides TiO_2 and ZrO_2. J. Photochem. Photobiol. A: Chem. 108 (1997): 179-185.

Nishida, S., Nagano, K., Phillips, L., March, S., and Anderson, M. Photocatalytic degradation of trichloroethylene in the gas phase using titanium dioxide pellets. J. Photochem. Photobiol. A: Chem. 70 (1993): 95-99.

Othmer, K. Encyclopedia of chemical technology. Vol. 6. 4 th ed. New York: A Wiley-Interscience Publication, John Wiley&Son, 1991.

Park, D., Zhang, J., Ikeue, K., Yamashita, H., Anpo, M. Photocatalytic oxidation of ethylene to CO_2 and H_2O on ultrafine powdered TiO_2 photocaalysts in the presence of O_2 and H_2O. J. Catal.185 (1999): 114-119.

Sato, T., Katakura, T.,Yin, S., Fujimoto, T., and Yabe, S. Synthesis and UV-shielding properties of calcia-doped ceria nanoparticles coated with amorphous silica. Solid State Ionics. 172 (2004): 377–382.

Seethawong, T., Suzuki, Y., and Yoshikawa, S. Synthesis, characterization, and photocatalytic activity for hydrogen evolution of nanocrystalline mesoporous

titania prepared by surfactant-assisted templating sol-gel process. J. Solid State chem. 178 (2005): 329-338.

Shang, J., Yao, W., Zhu, Y., and Wu, N. Structure and pohotocatalytic performances of glass/SnO_2/TiO_2 interface composite film. Appl. Catal. A: Gene. 257 (2004): 25-32.

Sinha, A.K., and Suzuki, K. Preparation and characterization of novel mesoporous ceria-titania. J. Phys. Chem. B. 109 (2005):1708-1714.

Sirisuk, A., Hill, C., and Anderson, M. Photocatalytic degradation of ethylene over thin films of titania supported on glass rings. Catal. Today. 54 (1999): 159-164.

Su, C., Hong, B., and Tseng, C. Sol-gel preparation and photocatalysis of titanium dioxide. Catal. Today. 96 (2004): 119-126.

Vinodgopal, K., Bedja, I., and Prashant, V.K. Nanostructured semiconductor films for photocatalysis. Photoelectrochemical behavior of SnO_2/TiO_2 composite systems and its role in photocatalytic degradation of a textile azo dye. Chem. Mater. 8 (1996): 2180-2187.

Vinodgopal, K., and Kamat, P. Enhanced rates of photocatalytic degradation of and azo dye using SnO_2/TiO_2 coupled semiconductor thin films. Environ. Sci. Technol. 29 (1995): 841-845.

Ward, D.A., and Ko, E.I. One-step synthesis and characterization of zirconia-sulfate aerogels as solid superacids. J. Catal. 150 (1994): 18-33.

Xie, C., Xu, Z., Yang, Q., Xue, B., Du, Y., and Zhang, J. Enhanced photocatalytic activity of titania-silica mixed oxide prepared via basic hydrolyzation. Mater. Sci. Eng. B. 112 (2004): 34-41.

Yamazaki, S., Fujinaga, N., and Araki, K. Effect of sulfate ions for so-gel synthesis of titania photocatalyst. Appl. Catal. A: Gen. 210 (2001): 97-102.

Yang, H., Lu, R., Shen, L., Song, L., Zhao, J., Wang, Z., and Wang, L. Preparation characterization and catalytic activity of sulfated zirconia–silica nanocrystalline catalysts. Mater. Lett. 57 (2003): 2572-2579.

Zhang, Y., Xiong, G., Yao, N., Yang, W., and Fu, X. Preparation of titania-based catalysts for formaldehyde photocatalytic oxidation from $TiCl_4$ by the sol-gel method. Catal. Today. 68 (2001): 89-95.

APPENDICES

APPENDIX A

CALCULATION OF THE CRYSTALLITE SIZE

Calculation of the crystallite size by Debye-Scherrer equation

The crystallite size was calculated from the width at half-height of the diffraction peak of XRD pattern using the Debye-Scherrer equation.

From Scherrer equation:

$$D = \frac{K\lambda}{\beta \cos \theta} \qquad \text{(A.1)}$$

where D = Crystallite size, Å

K = Crystallite-shape factor = 0.9

λ = X-ray wavelength, 1.5418 Å for CuKα

θ = Observed peak angle, degree

β = X-ray diffraction broadening, radian

The X-ray diffraction broadening (β) is the pure width of a powder diffraction, free of all broadening due to the experimental equipment. Standard α-alumina is used to observe the instrumental broadening since its crystallite size is larger than 2000 Å. The X-ray diffraction broadening (β) can be obtained by using Warren's formula.

From Warren's formula:

$$\beta^2 = B_M^2 - B_S^2 \qquad \text{(A.2)}$$

$$\beta = \sqrt{B_M^2 - B_S^2}$$

Where B_M = The measured peak width in radians at half peak height.

B_S = The corresponding width of a standard material.

Example: Calculation of the crystallite size of titania

The half-height width of 101 diffraction peak = 0.93125^{o}

= 0.01625 radian

The corresponding half-height width of peak of α-alumina = 0.004 radian

The pure width = $\sqrt{B_M^2 - B_S^2}$

= $\sqrt{0.01625^2 - 0.004^2}$

= 0.01577 radian

β = 0.01577radian

2θ = 25.56^{o}

θ = 12.78^{o}

λ = 1.5418 Å

The crystallite size = $\frac{0.9x\,1.5418}{0.01577\ \cos 12.78}$ = 90.15Å

= 9 nm

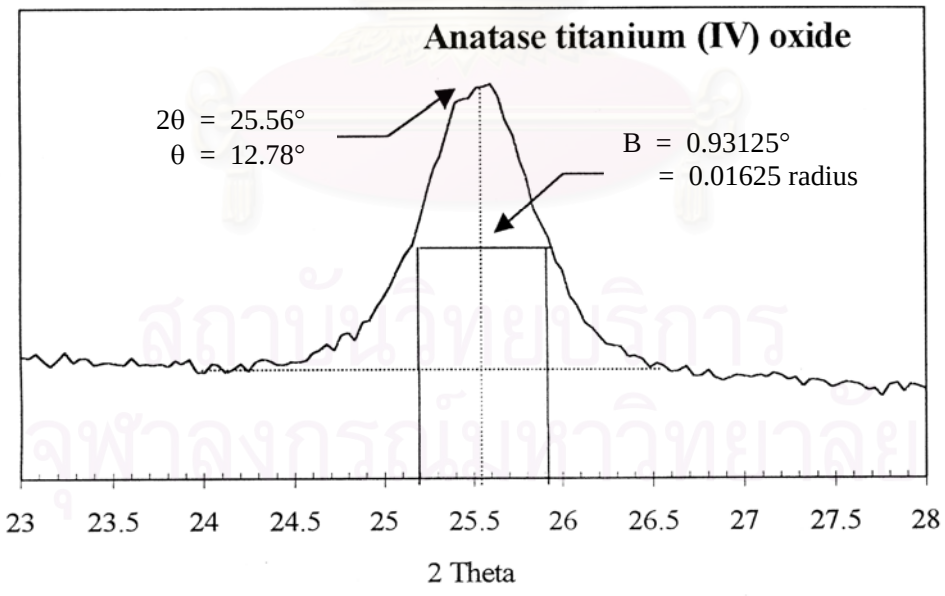

Figure A.1 The 101 diffraction peak of titania for calculation of the crystallite size

B

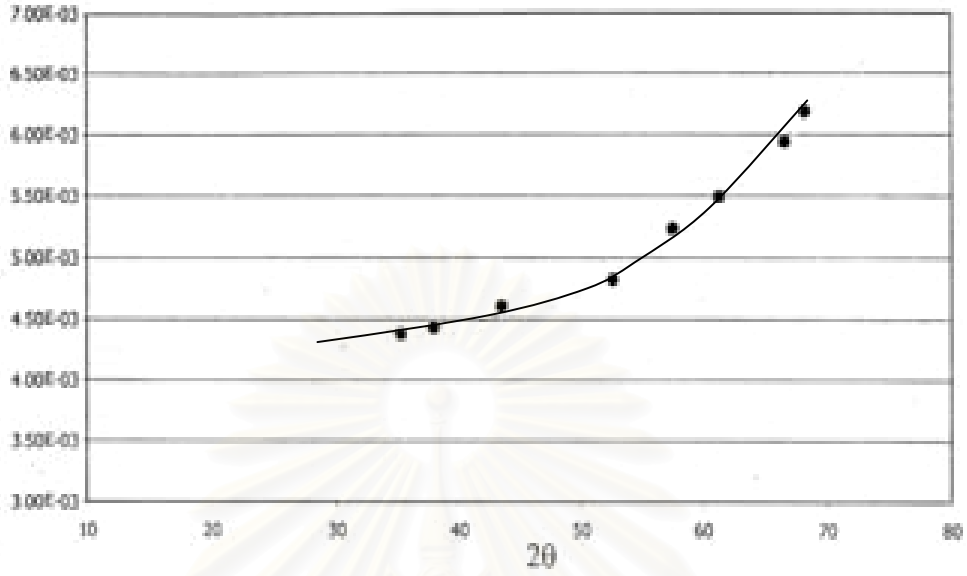

Figure A.2 The plot indicating the value of line broadening due to the equipment. The data were obtained by using α-alumina as standard.

APPENDIX B

THE OPERATING CONDITIONS OF GAS CHROMATOGRAPHY

The composition of hydrocarbons in the product stream was analyzed by a Shimadzu GC14B gas chromatograph equipped with a flame ionization detector. The operating conditions for each instrument are shown in the Table B.1.

Table B.1 The operating condition for gas chromatograph.

Gas Chromagraph	SHIMADZU GC-14B
Detector	FID
Column	VZ10
Carrier gas	H_2 (99.999%)
Carrier gas flow (ml/min)	30 cc/min
Column temperature	
- initial (^oC)	70
- final (^oC)	70
Injector temperature (^oC)	100
Detector temperature (^oC)	150
Current (mA)	-
Analysed gas	Hydrocarbon C_1-C_4

The calibration curve for calculation of composition of ethylene in reactor effluent was obtained and was shown in Figure B.1.

The VZ10 column was used with a gas chromatography equipped with a flame ionization detector to analyze the concentration of products including of ethylene.

Mole of ethylene as y-axis and area determined from gas chromatography as x-axis were plotted. The calibration curve of ethylene was illustrated in the following figure.

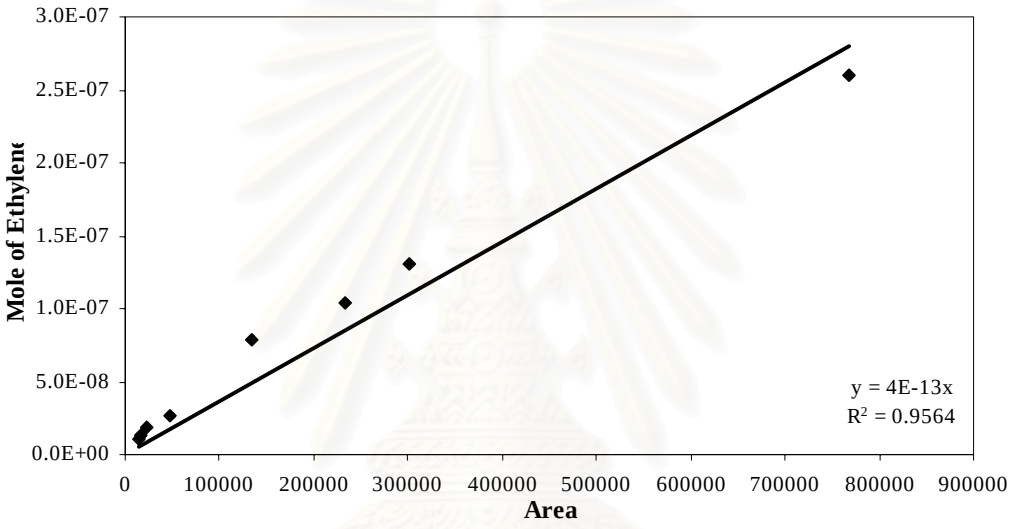

Figure B.1 The calibration curve of ethylene.

APPENDIX C

CALCULATION OF BET SURFACE AREA BY THE SINGLE POINT METHOD

From Brunauer-Emmett-Teller (BET) equation:

$$\frac{X}{V(1-X)} = \frac{1}{VmC} + \frac{(C-1)X}{VmC} \qquad (C.1)$$

Where: X = relative partial pressure of N_2, P/P_o

P_o = saturated vapor pressure of N_2 (or adsorbed gas) at the experimental temperature

P = equilibrium vapor pressure of N_2

V = volume of gas adsorbed at a pressure P; ml at the NTP/ g of sample

V_m = volume of gas adsorbed at monolayer, ml. at the NTP / g of sample

C = constant

Assume $C \rightarrow \infty$, then

$$\frac{X}{V(1-X)} = \frac{X}{Vm} \qquad (C.2)$$

$$Vm = V(1-P/P_o)$$

From the gas law,

$$\frac{P_b V}{273} = \frac{P_t V}{T} \qquad (C.3)$$

Where: V = constant volume

P_b = pressure at 0 ^oC

P_t = pressure at t ^oC

T = 273.15 + t, K

P_t = 1 atm and thus, P_b = (273.15 / T)

Partial pressure of Nitrogen:

$$P = \frac{[\text{Flow of } (He+N_2) - \text{Flow of } He]}{\text{Flow of } (He+N_2)} \quad (C.4)$$

$$= 0.3 \text{ atm}$$

N_2 saturated vapor pressure, P_o = 1.1 atm

$$p = P / P_o = P / 1.1 = 0.3/1.1 = 0.2727$$

How to measure V

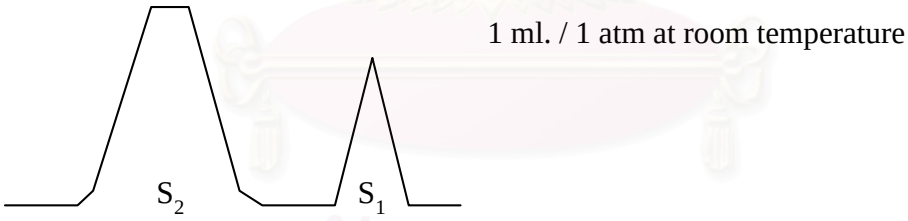

$$V = \frac{S_2}{S_1} \times \frac{1}{W} \times \frac{273.15}{T} \text{ ml. / g of catalyst} \quad (C.5)$$

Where, S_1 = Nitrogen 1 ml/1 atm of room temperature area

S_2 = Desorption of nitrogen area

W = Weight of the sample (g)

T = Room temperature (K)

Therefore,

$$Vm = \frac{S_2}{S_1} \times \frac{1}{W} \times \frac{273.15}{T} \quad X\ (1\text{-}p)$$

$$Vm = \frac{S_2}{S_1} \times \frac{1}{W} \times \frac{273.15}{T} \quad x\ 0.7273 \qquad (C.6)$$

Surface area of catalyst:

$$S = \frac{N\sigma V_m}{M}$$

Where, N = Avogadro number = 6.02×10^{23}

σ = area occupied by one molecule of adsorbed nitrogen = 16.2×10^{-20}

M = volume of one mole nitrogen = 22410 cm^3/mol

Then,

$$S = 4.352\ Vm$$

$$S = \frac{S_2}{S_1} \times \frac{1}{W} \times \frac{273.15}{T} \quad x\ 0.7273\ x\ 4.352$$

$$S = \frac{S_2}{S_1} \times \frac{1}{W} \times \frac{273.15}{T} \quad x\ 3.1582 \qquad (C.7)$$

APPENDIX D

LIST OF PUBLICATION

1. Ratchadaporn ninpetch, Akawat Sirisuk, "Effects of calcination conditions on properties and photocatalytic activities of titanium dioxide nanoparticles", Regional Symposium on Chemical Engineering 2004, Bangkok, Thailand, December 1-3, 2004, NS 230.

Effects of calcination conditions on properties and photocatalytic activities of titanium dioxide nanoparticles

*Ratchadaporn Ninpetch and Akawat Sirisuk**
Center of Excellence in Catalysis and Catalytic Reaction Engineering, Department of Chemical Engineering, Faculty of Engineering, Chulalongkorn University Bangkok,Thailand, 10330.
*Corresponding author (Email: akawat.s@eng.chula.ac.th)

ABSTRACT

Heterogeneous photocatalytic oxidation can be used for the degradation of volatile organic compounds (VOCs). This technique brings about the oxidation of airborne VOCs and produces carbon dioxide and water at room temperature in the presence of a semiconductor such as titania (TiO_2). Titania has been widely used as a photocatalyst because of its high photocatalytic activity, stability, low cost, and suitable band-gap energy. Titania nanoparticles were prepared via a sol-gel method using titanium isopropoxide as a precursor. Various characterization techniques were performed, including X-ray diffractometry and transmission electron microscopy. Effects of calcination conditions, namely, temperature and holding time in the furnace, on properties of titania nanoparticles were investigated. Both crystallite size and rutile content of titania increased as calcination temperature and holding time in the furnace increased. Titania nanoparticles were then employed as catalysts in photocatalytic oxidation of ethylene in gas phase. The reactor was a borosilicate glass tube with a diameter of 5 mm and a length of 27 cm and was surrounded by four 8 W fluorescent light bulbs. Reactor effluent was analyzed using a gas chromatograph in order to determine a conversion of ethylene.

Keywords: Titanium dioxide, Sol-gel method, Rutile content, Photo oxidation of ethylene.

INTRODUCTION

Titania nanoparticles in the anatase phase are active for photocatalytic degradation of several organic compounds in the treatment of wastewater and air pollutions. Photocatalytic performance of titania depends on particle size, specific surface area and crystal type [1-2]. In this work, we prepared titania nanoparticles by a sol-gel method using titanium isopropoxide as a precursor. Then photocatalytic activities of titania were measured using the photocatalyltic oxidation of ethylene in gas phase.

EXPERIMENTAL

Preparation of catalysts

Titanium dioxide was prepared using a sol-gel method [3]. Titanium isopropoxide was employed as a precursor. The precursor underwent controlled hydrolysis under acidic condition. Nitric acid was added to adjust the acidity of starting mixture. When titanium isopropoxide was slowly added to an aqueous solution of nitric acid, precipitation occurred immediately. The suspensions were stirred continuously at room temperature for about 3 days until clear sol was obtained. After that, the sol was dialyzed in a cellulose membrane with a molecular weight cutoff of 3500. The water was changed daily until the pH of the water reached 3.5. To remove solvents, the dialyzed sol was left in ambient atmosphere overnight and was dried at 110 °C. The resulting gel was then ground and sieved. Finally, titania nanoparticles were fired at four different temperatures, namely, 200 °C, 320 °C, 350 °C and 380 °C, for the duration of 1 to 3 hours.

Photocatalytic activity measurement

The photoreactor was a borosilicate glass tube with a diameter of 5 mm and a length of 27 cm and was surrounded by four 8 W fluorescent light bulbs. Approximately 0.4 g of titania was used in each experiment. The reactant was 0.1% (v/v) ethylene in air and was fed to the reactor at a rate of 15 ml/min. The temperature of the reactor under illumination was about 90 °C, as measured using a K-type thermocouple. The reactor effluent was sampled and analyzed using a gas chromatograph.

Characterization of catalysts

X-ray diffractometer (XRD) was employed to identify crystal phase of titania. The XRD patterns were then used to determine average crystallite sizes and contents of rutile phase of titania. Transmission electron microscope was used to inspect the shape and size of titania nanoparticles

RESULTS AND DISCUSSION

Table 1 summarizes conditions employed for calcination of different titania samples. X-ray diffractometry (XRD) was used to identify the crystal phase of titania. XRD patterns of two titania samples were displayed in Figure 1. In sample A200-1 only anatase phase was found while sample RA380-2 was a mixture of anatase and rutile phase. Average crystallite sizes of anatase and rutile (where applicable) were determined from the broadening of the characteristic peaks using Scherer's equation. Fraction of rutile phase present in the product was calculated from the ratio of the peak areas correponding the two phases [3]. The rutile content and average crystallite sizes of titania were also reported in Table 1.

Table 1. Summary of calcination conditions of titania samples and their properties.

Sample	Calcination temperature (ºC)	Calcination time (hr)	Rutile content (%)	Crystallite size of anatase (nm)	Crystallite size of rutile (nm)	Average conversion of ethylene
A200-1	200	1	0	4.69	n/a[b]	0.77
RA320-1	320	1	0.03	4.95	-[b]	0.61
RA350-1	350	1	1.93	5.99	-[b]	0.60
RA380-1	380	1	5.42	6.45	-	0.53
A200-2	200	2	0	5.11	n/a[b]	0.71
RA320-2	320	2	2.07	5.80	-[b]	0.60
RA350-2	350	2	4.09	6.40	-	0.52
RA380-2	380	2	7.89	7.31	9.77[b]	0.48
RA320-3	320	3	3.80	6.44	-[b]	0.54
RA350-3	350	3	6.03	6.88	-	0.47
RA380-3	380	3	14.45	7.38	10.05	0.41

Note: a. Specific surface area was determined from average crystallite size obtained from XRD patterns.
b. Crystallite size of rutile could not be determined because the observed rutile speaks were too small.

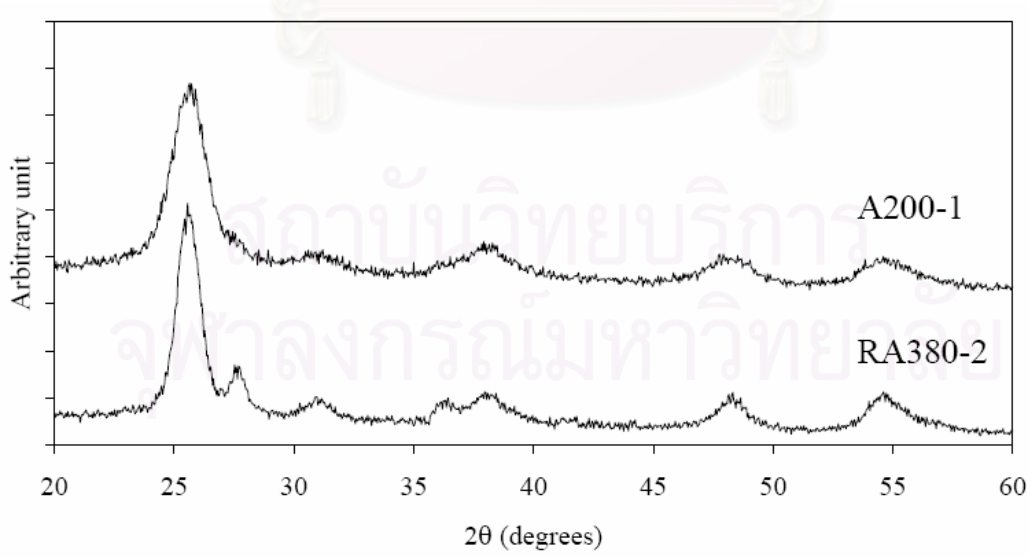

Figure 1. The XRD patterns of titania that was fired at 200 °C for one hour (A200-1) and another that was fired at 380 °C for 2 hour

Transmission electron microscope (TEM) was employed to investigate the shape and size of titania nanoparticles. Figure 2 shows the TEM image obtained for titania that was fired at 350 °C for 2 hours. The shape of the particles appeared to be irregular. Similar morphology was found for other titania samples prepared.

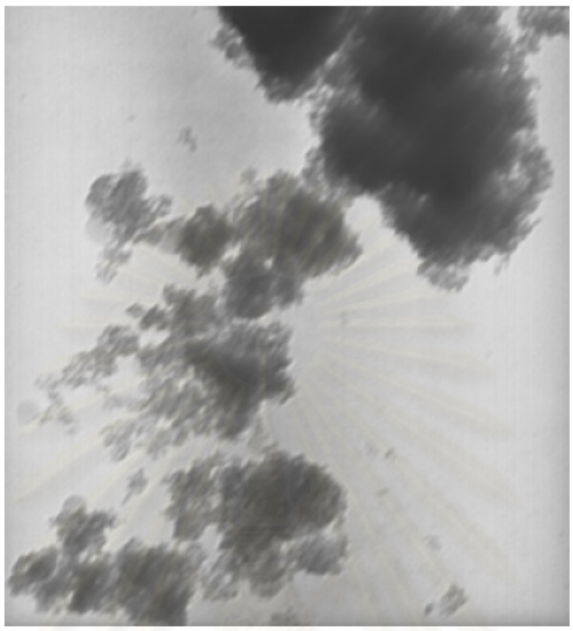

Figure 2. The TEM image of titania nanoparticles that were fired at 350 °C for 2 hours.

From Table 1, as calcination temperature of titania increased, both crystallite size and rutile content of titania increased. Similarly, the same trends were observed when holding time in the furnace was increased. Titania nanoparticles were used as catalysts in photocatalytic oxidation of ethylene. The conversion of ethylene achieved from titania was displayed in Table 1. When average crystallite size of anatase phase in the sample increased, either from higher calcination temperature or longer holding time, the achieved conversion of ethylene decreased. As titania nanoparticles become larger, specific surface area of the particles decreases and hence a fewer number of active surface sites available for the reaction. Zhang et al. [5] reported that the photocatalytic activity of nanocrystalline titania photocatalyst does not in crease monotonically with decreasing particle size because benefits from high surface area are offset by the increased recombination rate of electron-hole pairs at the surface of the nanoparticles. Nevertheless the offset was not observed in our experiments (see Figure 3). Another factor that may contribute to the decrease of photocatalytic activity as calcination temperature or holding time in the furnace increased was fraction of rutile phase present in the samples. Figure 4 shows the conversion of ethylene as a function of rutile content in the samples. Since rutile has lower or no photocatalytic activity [6-8], increase in rutile content in the sample should reduce the overall activity of titania photocatalyst. Our finding contradicts the study conducted by Wu et al. [6], which observed a synergetic effect between the anatase and rutile phase and reported the optimal ratio of anatase to rutile to be between 88/12 and 85/15, depending on reaction.

CONCLUSIONS

Titanium dioxide nanoparticles were prepared using a sol-gel method. Variables in calcinations process, i.e., temperature and holding time in the furnace, were studied. Increase in either temperature or holding time resulted in titania that had larger crystallite size and higher rutile content. Photocatalytic activities of titania decreased as calcinations temperature and holding time in the furnace increased. The decrease may be attributed to lower specific surface area of larger crystals and higher amount of rutile phase present in titania [9].

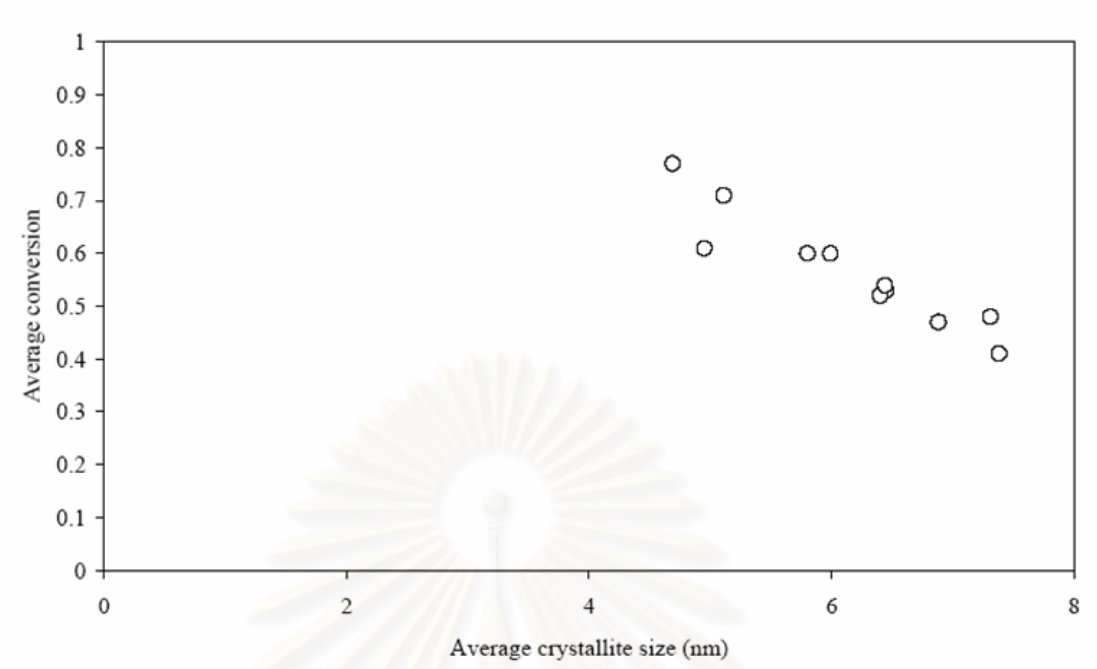

Figure 3. Average conversion of ethylene achieved in photocatalytic oxidation over titanium dioxide nanoparticles as a function of average crystallite size of anatase in the sample.

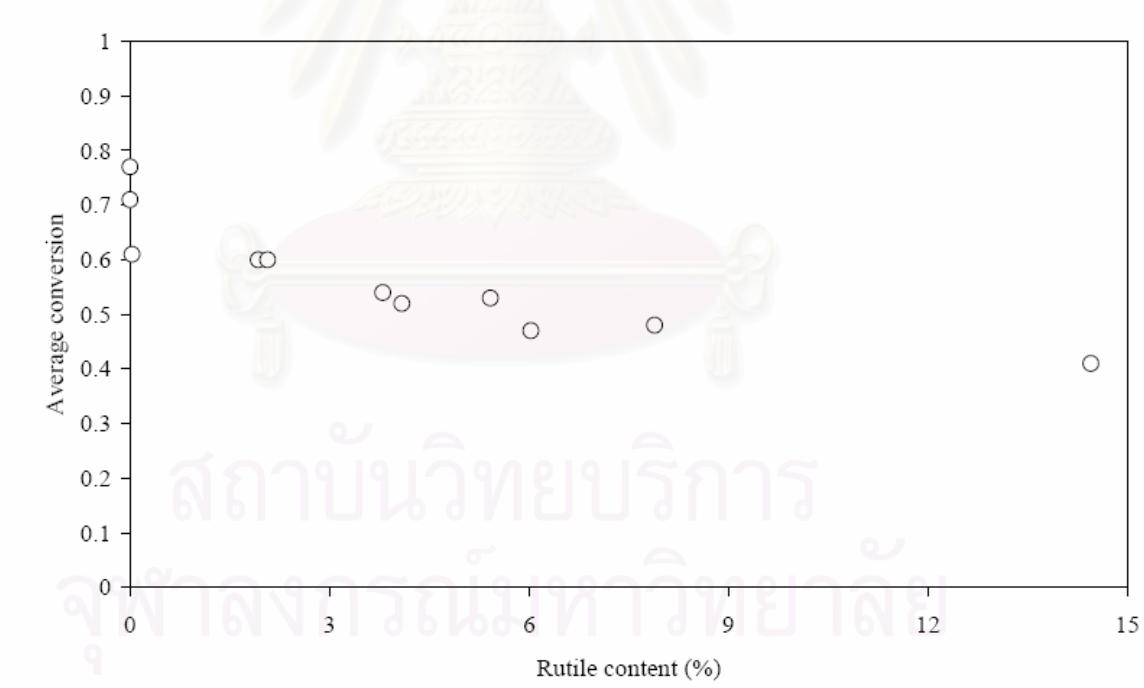

Figure 4. Average conversion of ethylene achieved in photocatalytic oxidation over titanium dioxide nanoparticles as a function of fraction of rutile phase present in the sample.

ACKNOWLEDGMENT

We would like to acknowledge financial supports from National Research Council of Thailand, Thailand Research Fund, Commissions on Higher Education, and Graduate School of Chulongkorn University.

REFERENCES

[1] Gan, L. and Zhang, Q., 'Effects of Am, K., 'Effect of Sulfate Ions for Sol-Gel Synthesis of Titania Photocatalyst', *Applied catalysis A: General*, 210, pp 97-102, (2001).

[2] Yamazaki, S., Fujinaga, N., and Araki, K., 'Effect of Sulfate Ions for Sol-Gel Synthesis of Titania Photocatalyst', *Applied catalysis A: General*, 210, pp 97-102, (2001).

[3] Fu, X., Clark, L.A., Yang, Q., and Anderson, M.A., 'Enhanced Photocatalytic Performance of Titania-Based Binary Metal Oxides: TiO_2/SiO_2 and TiO_2/ZrO_2', *Environmental Science and Technology*, 30, pp 647-653, (1996).

[4] Zhang, Q., Gao, L., and Guo, J., 'Effects of Calcinations on the Photocatalytic Properties of Nanosized TiO_2 Powders Prepared by $TiCl_4$ Hydrolysis', *Applied Catalysis B: Enviromental*, 26, pp 207-215, (2000).

[5] Zhang, Z., Wang, C., Zakaria, R., Ying, J.Y., 'Role of Particle Size in Nanocrystalline TiO_2-Based Photocatalysts', *Journal of Physical Chemistry B*, 102, pp 10871-10878, (1998).

[6] Wu, C., Yue, Y., Deng, X., Hua, W., and Gao, Z., 'Investigation on the Synergetic Effect between anatase and Rutile Nanoparticles in Gas-Phase Photocatalytic Oxidations', *Catalysis Today*, 93-95, pp 863-869, (2004).

[7] Cheng, S., Tsai, S., and Lee, Y., 'Photocatalytic Decomposition of Phenol over Titanium Dioxide of Various Structures', *Catalysis Today*, 26, pp 87-96, (1995).

[8] Agrios, A.G., Gray, K.A., and Weitz, E., 'Photocatalytic Transformation of 2,4,5-Trichlorophenol on TiO_2 under Sub-Band-Gap Illumination', *Langmuir*, 19, pp 1402-1409, (2003).

[9] Yamazaki-Nishida, S., Nagano, K.J., Phillips, L.A., Carvera-March, S., and Anderson, M.A., 'Photocatalytic Degradation of Trichloroethylen in the Gas Phase Using Titanium Dioxide Pellets', *Journal of Photochemistry and Photobiology A: Chemistry*, 70, pp 95-99, (1993). orphous Contents and Particle Size on the Photocatalytic Properties of Titania', *Scripta Materialia* , 44, pp 1195-1198, (2001).

VITA

Miss Ratchadaporn Ninpetch was born on September 23, 1974 in Suphanburi Province, Thailand. She received the Bachelor Degree of Chemical Engineering from Faculty of Engineering, Mahanakorn University of Technology in 2000. In June 2003, she started her graduate study at department of Chemical Engineering, Chulalongkorn University.